Mon. Not. R. Astron. Soc. **305,** 190–210 (1999)

# The symbiotic binary system RX Puppis: a possible recurrent nova with a Mira companion

Joanna Mikołajewska,[1⋆] Estela Brandi,[2†] Warren Hack,[3] Patricia A. Whitelock,[4] Rodolfo Barba,[2‡] Lia Garcia[2] and Freddy Marang[4]

[1]*Copernicus Astronomical Center, Bartycka 18, PL 00-716 Warsaw, Poland*
[2]*Facultad de Ciencias Astronómicas y Geofísicas, Universidad Nacional de la Plata, Paseo del Bosque S/N, 1900 La Plata, Argentina*
[3]*Space Telescope Science Institute, 3700 San Martin Drive, Baltimore, MD 21218, USA*
[4]*South African Astronomical Observatory, PO Box 9, 7935 Observatory, South Africa*

Accepted 1998 December 21. Received 1998 December 10; in original form 1998 October 5

**ABSTRACT**

We present an analysis of photometric and spectroscopic observations of the symbiotic binary system RX Pup with the aim of developing a reliable binary model for the system and identifying mechanisms responsible for its spectacular activity. The binary is composed of a long-period Mira variable surrounded by a thick dust shell and a hot $\sim 0.8\,M_{\odot}$ white dwarf companion. The hot component produces practically all activity observed in the UV, optical and radio range, while variable obscuration of the Mira by circumstellar dust is responsible for long-term changes in the near-infrared magnitudes. The observations show that RX Pup underwent a nova-like eruption during the last three decades. The hot component contracted in radius at roughly constant luminosity from 1975 to 1986, and was the source of a strong stellar wind, which prevented it from accreting material lost in the Mira wind. Around 1988/9 the hot component turned over in the Hertzsprung–Russell (HR) diagram and by 1991 its luminosity had faded by a factor of $\sim$30 with respect to the maximum plateau value and the hot wind had practically ceased. By 1995 the nova remnant started to accrete material from the Mira wind, as indicated by a general increase in intensity of the optical continuum and H I emission. The quiescent spectrum resembles the quiescent spectra of symbiotic recurrent novae, and its intensity indicates that the hot component must accrete as much as $\sim$1 per cent of the Mira wind, which is more or less the amount predicted by Bondi–Hoyle theory. The earliest observational records from the 1890s suggest that another nova-like eruption of RX Pup occurred around 1894.

**Key words:** binaries: symbiotic – circumstellar matter – stars: individual: RX Pup – stars: mass-loss – novae, cataclysmic variables.

## 1 INTRODUCTION

Despite numerous papers describing the multifrequency behaviour of the symbiotic binary RX Pup (HD 69190), and several attempts to determine the physical mechanisms responsible for its spectral peregrinations, it remains one of the most puzzling symbiotic systems ever found.

Based on the peculiar emission-line spectrum, as well as irregular photometric variability, RX Pup was initially placed among the irregular variable stars related to $\eta$ Car or R CrB (Pickering 1897, 1914; Payne-Gaposchkin & Gaposchkin 1938). In 1941 the star was characterized by a continuous spectrum confined to the yellow and red region and very intense high-excitation emission lines of [Fe VII], [Ne V], [Fe VI] and [Ca VII], similar to those observed in CI Cyg and AX Per, which led Swings & Struve (1941) to classify RX Pup as a symbiotic star. The presence of an evolved red giant in RX Pup was not established until the 1970s, when M-type absorption features were observed for the first time (Barton, Phillips & Allen 1979; Andrillat 1982), while extensive photometric observations in the near-infrared demonstrated that the system contains a long-period variable with $P \approx 580$ d (Feast, Robertson & Catchpole 1977; Whitelock et al. 1983a, hereafter W83). Direct evidence for the binary nature of RX Pup has been provided by the detection of a hot UV continuum source with the *International Ultraviolet Explorer* (*IUE*) satellite (Kafatos, Michalitsianos & Feibelman 1982 and Kafatos, Michalitsianos & Fahey 1985, hereafter K82 and K85, respectively).

⋆E-mail: mikolaj@camk.edu.pl
†Member of the Carrera del Investigator CIC – Provincia de Buenos Aires.
‡Member of the Carrera del Investigator CONICET.

Because of the large volume of observational data available and the relatively recent onset of activity, RX Pup has been regarded as a key object in unravelling the nature of symbiotic Miras, especially as it is one of the brightest symbiotics at radio and infrared wavelengths. The models proposed to provide the hot component luminosity and to explain the observed activity involve – as is usual for symbiotic binaries – either thermonuclear runaway on the surface of a wind-accreting white dwarf (Allen & Wright 1988, hereafter AW88) or variable disc-accretion on to a compact star (Ivison & Seaquist 1994, hereafter IS94; see also K85).

In the AW88 model a low-mass white dwarf slowly accretes hydrogen-rich material from the wind of a distant Mira companion until a thermonuclear runaway occurs. Such a flash, especially for a low-mass white dwarf, can last for many decades; the hot component of RX Pup now has a luminosity close to the Eddington value. The observed periods of low and high excitation were postulated to be caused by variable mass loss from the white dwarf, while the low reddening reported during the low-excitation stage was attributed to the close proximity of a shock front (where the wind from the hot component collides with the wind from the Mira) to the Mira.

IS94 proposed an alternative scenario in which, during some portion of the orbital period, the Mira fills its tidal lobe and is gravitationally stripped of its dusty envelope; as a result the circumstellar reddening is significantly reduced. An accretion disc or torus forms, causing the UV radiation of the hot companion to be reprocessed. As in the AW88 model, the bolometric luminosity of the compact star remains unchanged as it goes from high- to low-excitation phases. In this model the flattening of the radio spectrum and the disappearance of the high-excitation emission lines result from cooling of the radiation field in the orbital plane.

Unfortunately, both models have some significant difficulties when confronted with existing observations. In particular, both AW88 and IS94 assumed that RX Pup drifts between two extreme (low- and high-excitation) states without major changes in its bolometric luminosity. In fact there are major differences between the low-excitation phases reported in 1949/51 (Henize 1976) and the late 1960s, when the optical continuum was very faint ($m_v \sim 12.5$, $m_{pg} = 13.5$ in 1968 February; Sanduleak & Stephenson 1973) and the low-excitation phase observed in 1972–1978. The latter was characterized by a significant increase in the optical brightness ($V \sim 9$–$8$, $B \sim 9$–$10$) which strongly suggests intrinsic variability of the hot source.

This paper contains an analysis of photometric and spectroscopic observations of RX Pup made with the objective of developing a reliable binary model and identifying the causes of its unusual variability. A description of the data base is given in Section 2, analysed in Section 3 and the results discussed in Section 4, while Section 5 contains a brief summary and conclusion.

## 2 OBSERVATIONS

### 2.1 Ultraviolet spectroscopy

Various observers acquired ultraviolet spectra of RX Pup throughout 1978–1993 with *IUE*. These spectra covered a significant part of the last phase of activity. Table 1 summarizes the relevant parameters for these observations, including the Julian date (JD), spectrum identifier (*L* and *H* indicate low- and high-resolution data for short-wavelength – SWP – and long-wavelength – LWR and LWP – exposures) and visual magnitudes derived from Fine Error Sensor (FES) counts. Most of the *IUE* data, in particular the low-resolution SWP spectra taken prior to 1980 September and after 1986 May as well as practically all LWR/LWP spectra, have not been published.

**Table 1.** Journal of *IUE* observations.

| Date | JD 24... | SWP | LWR/P | $m_v$ |
|---|---|---|---|---|
| 1978, Sep 18 | 43770 | 2684 L | 2395 L | |
| 1979, Jun 30 | 44055 | 5680 L | 4922 L | 9.2 |
| 1979, Jul 17 | 44072 | 5835 L | 5081 L | 9.3 |
| 1979, Jul 19 | 44074 | | 5106 L | 9.3 |
| 1980, Apr 15 | 44345 | 8762 L | 7505 L | 9.7 |
| 1980, Sep 21 | 44503 | 10189 L | 8856 L | 9.8 |
| | | 10190 L | | |
| | | 10191 H | | |
| 1981, Jun 11 | 44767 | 14239 L | 10830 L | 10.2 |
| | | 14240 H | 10832 L | |
| 1982, Mar 22 | 45051 | 16597 H | 12837 H | 10.4 |
| | | 16598 L | 12836 L | |
| 1983, Oct 30 | 45638 | 21402 H | 2177 H | 11.0 |
| | | 21403 L | 2176 L | |
| 1984, Mar 11 | 45771 | 22461 H | | 11.0 |
| | | 22462 L | 2924 L | |
| 1986, May 8 | 46559 | 28270 H | | 11.2 |
| | | 28271 L | 8160 L | |
| | | | 8161 L | |
| | | | 8162 L | |
| | | | 8163 L | |
| 1986, May 9 | 46560 | 28278 H | 8170 H | 11.2 |
| | | 28279 L | 8164 L | |
| | | 28284 L | 8165 L | |
| | | | 8166 L | |
| | | | 8167 L | |
| | | | 8168 L | |
| | | | 8169 L | |
| 1987, Jul 3 | 46980 | 31285 H | | 11.3 |
| 1988, Oct 24 | 47459 | 34594 L | 14309 L | 11.5 |
| | | 34595 H | 14310 H | |
| 1989, May 20 | 47667 | 36307 L | 15552 L | 11.7 |
| | | 36308 L | | |
| 1991, Mar 29 | 48345 | 41209 L | 20008 L | 12.2 |
| 1993, May 27 | 49135 | 47757 L | 25611 L | |
| 1993, May 28 | 49136 | | 25615 L | |

The low-resolution *IUE* spectra were transformed into absolute fluxes using standard calibrations (Holm et al. 1982) and the LWR spectra were corrected for sensitivity degradation (Clavel, Gilmozzi & Prieto 1986). The high-resolution spectra were calibrated as suggested by Cassatella, Ponz & Selvelli (1982). Table 2 lists emission-line fluxes derived by fitting Gaussian profiles as a function of Julian date; these estimates have errors of ±10 per cent for strong emission lines and ±25 per cent for weaker lines. Examples of ultraviolet spectra are shown in Fig. 1.

### 2.2 *HST* observations

We carried out *HST* observations using the FOC/96 camera on 1991 March 12 (JD 244 8328). FOC images were taken with the F501N ([O III] 5007 Å) filter and the near-UV objective prism (NUVOP) crossed with the F195W filter. The direct image taken with the F501N filter provided measurements of the undispersed position of a star for the analysis of the prism observation.

Unfortunately, the FOC images are not conclusive regarding the point-like nature of RX Pup. Those images without the prisms in place are, unfortunately, saturated, leaving only the very extended halo to hint at the point-like nature of the object. The best we can

**Table 2.** Ultraviolet emission-line fluxes in RX Pup in units of $10^{-12}$ erg cm$^{-2}$ s$^{-1}$.

| JD 24... | 44055 | 44072 | 44345 | 44503 | 44767 | 45051 | 45638 | 45771 | 46559 | 47459 | 47667 | 48345 |
|---|---|---|---|---|---|---|---|---|---|---|---|---|
| N v 1240 | | | | | 0.3 | 0.5 | 0.7 | 0.9 | 1.6 | 0.6 | 0.7 | |
| O i 1304 | 0.8 | 1.2: | 1.0 | 0.7 | 0.8 | 1.3: | 0.3 | 0.3 | 0.3 | 0.1 | | |
| Si iv 1394 | 0.6: | 0.5: | 0.7 | 0.7 | 0.8 | 0.8 | 0.7 | 0.7 | 0.7 | 0.4 | 0.3 | |
| O iv] 1403 | 0.5: | 0.8 | 1.0 | 0.8 | 1.6 | 2.6 | 2.2 | 3.5 | 2.2 | 1.1 | 1.2 | |
| N iv] 1487 | 0.9 | 1.4 | 2.7 | 2.4 | 3.4 | 3.5 | 3.1 | 3.3 | 3.1 | 1.3 | 1.3 | |
| C iv 1550 | 7.2 | 8.5 | 10.7 | 10.6 | 11.7 | 11.3 | 9.5 | 8.7 | 8.5 | 6.5 | 6.2 | |
| [Ne v] 1575 | | | 0.3 | 0.3 | 0.3 | 0.3 | 0.4 | | 0.3 | 0.3 | 0.2 | |
| [Ne iv] 1602 | | | 0.6 | | 0.4 | 0.6 | 0.5 | | | 0.5 | 0.4 | |
| He ii 1640 | 0.7 | 1.1 | 3.5 | 3.9 | 5.3 | 5.6 | 6.0 | 5.8 | 5.1 | 4.1 | 3.5 | |
| O iii] 1664 | 2.3 | 2.9 | 5.9 | 5.7 | 5.6 | 5.1 | 4.0 | 3.8 | 3.1 | 1.5 | 1.1 | |
| N iv 1719 | | | | | 0.2 | 0.2 | | 0.3 | 0.2 | 0.1 | | |
| N iii] 1750 | 1.8 | 2.7 | 3.0 | 3.6 | 3.7 | 3.4 | 2.7 | 2.5 | 2.0 | 1.2 | 1.1 | |
| Si ii 1818 | 0.2 | 0.3 | 0.5 | 0.5 | 0.4 | 0.5 | 0.5 | | | 0.2 | 0.2 | |
| Si iii] 1892 | 2.6 | 2.9 | 3.7 | 3.7 | 3.8 | 3.6 | 2.6 | 2.4 | 2.0 | 1.0 | 0.8 | |
| C iii] 1909 | 4.1 | 4.5 | 8.0 | 8.5 | 10.0 | 10.1 | 8.3 | 8.5 | 5.9 | 3.8 | 3.4 | |
| He ii 2511, Fe ii 2513 | 1.1 | 1.4 | 1.5 | 0.9 | 1.0 | 1.0 | 0.6 | 0.7 | 0.5 | 0.2 | 0.3 | |
| Al ii] 2669 | | | | 1.0 | 0.8 | 0.6 | 0.3 | 0.3 | 0.3 | 0.1 | 0.2 | |
| He ii 2733 | | | 0.8 | 0.8 | 0.8 | 0.6 | 0.6 | 0.6 | 0.6 | 0.3 | 0.3 | |
| Fe ii 2756 | | | | 0.6 | | 0.4 | | 0.4 | 0.3 | | 0.1 | 0.1 |
| Fe ii 2774 | 0.7 | 1.3 | 1.0 | 1.2 | 1.2 | 0.7 | 0.3 | 0.3 | | | | |
| [Mg v] 2783 | | | | | | | 0.3 | 0.3 | 1.0 | 1.4 | 1.0 | |
| Mg ii 2800 | 5.3 | 5.5 | 3.5 | 3.1 | 8.9 | 9.7 | 7.9 | 4.5 | 3.6 | 2.1 | 1.9 | 0.5 |
| [Fe iv] 2829 | | 0.6: | 0.7 | 0.3 | | 0.5 | 0.6 | 0.7 | 0.6 | 0.4 | 0.4 | |
| O iii 2838 | | | 0.3 | 1.8 | 2.2 | 1.7 | 1.9 | 1.8 | 1.9 | 1.0 | 0.9 | |
| Fe ii 2847 | 4.0 | 3.1 | 1.9 | 0.9 | 1.5 | 1.6 | 1.0 | 0.7 | 0.4 | | 0.1 | |
| Fe ii 2859 | | 1.2: | | | 0.5 | 1.1 | 0.5 | 0.4 | 0.3 | | 0.3 | |
| [Mg v] 2928 | | | | | | | | | 0.7 | 0.5 | 0.4 | |
| Mg ii 2936 | 0.6 | 1.0 | | 0.4 | 0.7 | 0.6 | | | | | | |
| [Ne v] 2973 | | | | | | | 0.5 | 0.3 | 0.5 | 0.4 | 0.2 | |
| O iii 3025 | | | | 0.8 | 0.8 | 0.8 | 0.8 | 0.8 | 0.9 | 0.5 | 0.3 | |
| O iii 3047 | | | | 1.9 | 2.2 | 1.8 | 1.1 | 1.8 | 1.7 | 0.9 | 0.8 | |
| Ti ii 3079 | 1.4 | 1.6 | 1.2 | | 0.9 | 0.4 | | | | | 0.3 | |
| O iii 3133 | 1.9 | 2.1 | 6.5 | 5.1 | 8.3 | 9.3 | 10.4 | 10.0 | 9.1 | 5.4 | 4.7 | |

There were no measurable emission lines present on JD 244 3770 and JD 244 9135 (see also Section 3.1.2).

say is that the FOC images place an uncertain upper limit to the size of RX Pup of approximately 0.2 arcsec. Additional UV and optical images taken late in 1993 with the FOC do not provide substantive evidence of any extended features, down to an upper limit of 0.06 arcsec. However, the low signal-to-noise ratio in the images and the lack of information regarding the actual focus of *HST* and FOC at the time of the observations preclude making any definitive conclusions.

A relatively long exposure time, of 900 s, was required for the objective prism image to give sufficiently high signal-to-noise ratio across the full spectral range from 1750–5500 Å. The FOC detectors are count-rate limited (unlike CCDs) so a 512 pixel × 512 pixel format was used to maintain linearity for the star with count rates up to about 0.5 count s$^{-1}$ pixel$^{-1}$. This format provides an $11 \times 11$ arcsec$^2$ field of view, with pixel sizes of $0.022 \times 0.022$ arcsec$^2$.

The objective prism image taken with PRISM2 + F195W (NUVOP) provided low-resolution spectroscopy of RX Pup (Fig. 2). The peak count rates in the objective prism image were less than 0.2 count s$^{-1}$ pixel$^{-1}$, ensuring photometric linearity throughout the entire observed spectral region. This observation gave a signal-to-noise ratio ranging from $\approx 2$ at 1800 Å to $\approx 14$ at 4000 Å.

All of the observations were flat-fielded and geometrically corrected using the standard FOC pipeline calibrations described in detail the FOC Instrument Handbook (Nota et al. 1996, henceforth FOCIH). The dispersed images taken with the objective prisms are aligned with the visible wavelengths on the lower end and the UV wavelengths at the upper end. The NUVOP image had a resolution of 40 Å pixel$^{-1}$ at 5000 Å and 0.5 Å pixel$^{-1}$ at 1700 Å extending across the entire image (512 pixels).

Seven-pixel (0.15 arcsec) wide regions centred on the peak of the spectrum were extracted, and the contribution from all the pixels summed to provide the raw spectrum. This raw spectrum was wavelength-calibrated by applying the latest dispersion relation for each prism as given in the FOCIH. The zero-point for the conversion was based on the position of each star in the F501N image, with the distance along the spectrum from that zero-point determining the wavelength of the spectrum. Flux-calibrating the spectrum required some knowledge of the percentage of total flux from the source that was contained in the spectrum to recover all the flux from the source. This percentage is based on the width of the extraction used for the spectrum, which was 7 pixels. An empirical relationship for this percentage was determined using spectrophotometric standards and the method reported in the FOCIH This relationship served as the initial estimate for our reductions. With an estimate of the total flux contained in the extraction, the raw spectrum was then converted from counts to flux units by dividing out the FOC and filter sensitivities using software written as part of the Space Telescope Science Data Analysis System (STSDAS) and described in the FOCIH.

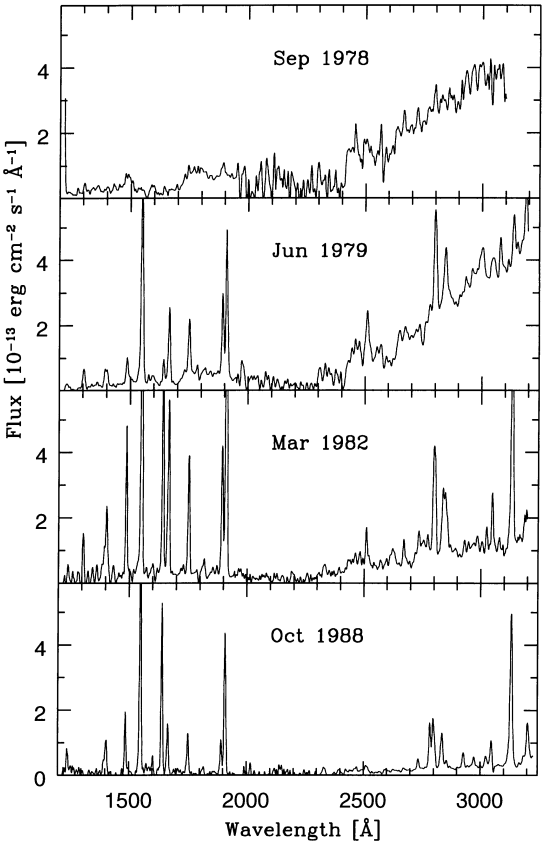


**Figure 1.** *IUE* low-resolution spectra of RX Pup taken in 1978–1988. The spectra show the gradual decline of the UV continuum and the evolution of emission-line fluxes.

### 2.3 Optical spectroscopy

The optical spectra were taken during 4 observing runs, in 1990 November (JD 244 8200), 1991 April (JD 244 8352), 1995 June (JD 244 9890) and 1996 March (JD 245 0167), with the 2.15-m telescope of Complejo Astronómico El Leoncito (CASLEO) at San Juan, Argentina. In 1990 and 1991 the Boller & Chivens (B&C) Cassegrain spectrograph and a Reticon photon-counting system known as the 'Z-Machine' was used. The 'Z-Machine' is a double aperture detector which permits one to observe simultaneously the sky and the target plus sky. A translation of the object from one aperture to the other is made at mid exposure for each observation, and the combination of these two data sets gives a sky-free spectrum. An aperture of $5 \times 3$ arcsec$^2$ was used. The 1200 line mm$^{-1}$ grating gives two wavelength ranges of about 4400–5100 and 5800–7200 Å, with dispersions of 0.5 and 1 Å pixel$^{-1}$, respectively. A spectral resolution of at least 4100 and 2700 in the two spectral regions, respectively, is indicated by measurements of the full width at half maximum (FWHM) of arc lines. In 1995 and 1996, the spectra were taken with the REOSC echelle spectrograph at a resolution of 15 000, and recorded with a TEK $1024 \times 1024$ CCD. The reduction of the 'Z-Machine' spectra was carried out with the IHAP image processing software. Wavelength calibration was performed using the He–Ar–Ne lamps with reference exposures obtained immediately before and after each stellar exposure, at the same sky position. Flat-field exposures were also done and a mean value was used in the reduction procedure. The echelle spectra were reduced with standard IRAF packages, CCDRED and ONEDSPEC.

To obtain the flux calibration, standard stars from Stone & Baldwin (1983) and Baldwin & Stone (1984) were observed each night. A comparison of the spectra of the standards suggests that the flux calibration errors are about 15 per cent for the 'Z-Machine' and 20 per cent in the central part of each order for the REOSC echelle images, respectively.

An additional optical spectrum was obtained in 1991 May (JD 244 8385), with the 1.5-m telescope of ESO at La Silla, and the B&C spectrograph (used in the range 4300–6900 Å) equipped with a CCD ($512 \times 1024$ pixel$^2$). The spectrum was reduced following the IHAP routines, using flat-field exposures, HeAr wavelength calibration spectra and standard stars (Hayes & Latham 1975) observed each night for flux calibrations. The photometric calibrations are accurate to 10–20 per cent.

Emission-line fluxes derived by fitting Gaussian profiles are listed in Table 3. These data have uncertainties of ~10–15 per cent for strong lines and ~20–30 per cent for weak lines or noisy spectra. Examples are shown in Fig. 3.

### 2.4 Photometry

*JHKL* broad-band photometry (1.25, 1.65, 2.2, 3.45 μm) was obtained with the Mk II infrared photometer on the 0.75-m telescope at SAAO, Sutherland (see Carter 1990 for details about the system). Some of the early data have been published (W83; Whitelock et al. 1984, hereafter W84), although the values given

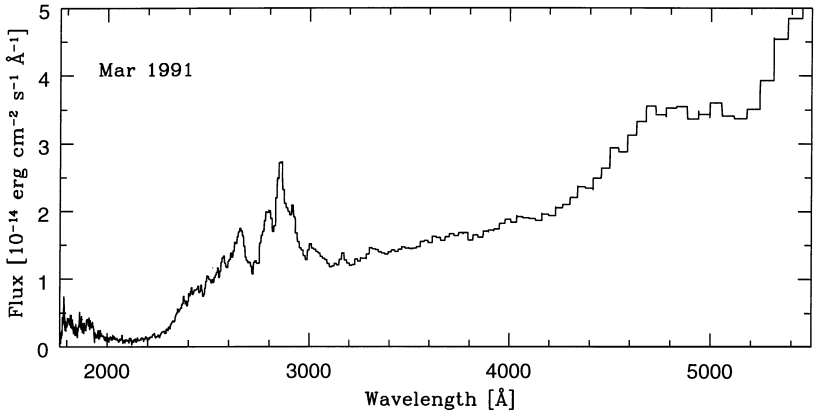


**Figure 2.** *HST* low-resolution spectrum of RX Pup taken on 1991 March 12.

**Table 3.** Optical emission-line fluxes in units of $10^{-13}$ erg cm s$^{-1}$.

| JD 24... | 48200 | 48352 | 48385 | 49890 | 50167 | JD 24... | 48200 | 48352 | 48385 | 49890 | 50167 |
|---|---|---|---|---|---|---|---|---|---|---|---|
| [Fe II] 4244 | | | | | 1.0 | Fe II 5317 | | | 1.5 | 3.3 | 2.7 |
| C II 4267 | | | | | 1.3 | [Fe II], Fe II 5362 | | | 0.7 | 2.2 | 1.7 |
| [Fe II] 4287 | | | | | 1.8 | [Fe II], Fe II 5413 | | | 1.1 | 1.2 | 1.5 |
| H$\gamma$ 4340 | | | 5.5 | | 6.5 | Fe II 5535 | | | 0.6 | 2.3 | 2.2 |
| [O III] 4363 | | | 2.3 | | 0.7 | [O I] 5577 | | | 0.5 | 0.5: | 1.0: |
| He I, Fe II 4387 | | | 0.5 | | 0.6 | [N II] 5755 | | | 8.0 | 1.0 | 0.7 |
| [Fe II] 4414 | 1.6 | 0.8 | 1.4 | | 1.0 | He I 5876 | 61.0 | 4.9 | 4.2 | 0.1: | 0.4 |
| Fe II 4417 | | 1.0 | | | 0.7 | Na I 5890 | | 3.7 | 3.1 | abs | abs |
| [Fe II] 4452 | | 0.4 | 0.7 | | 1.1 | Na I 5896 | | 2.6 | 2.8 | abs | abs |
| [Fe II] 4458 | | 0.5 | 0.6 | | 0.4 | Fe II 5991 | | | 0.6 | 3.0 | 3.9 |
| He I, Fe II 4472 | 3.1 | 1.1 | 1.1 | | 0.3 | Fe II 6084 | | | 0.4 | 2.3 | 1.9 |
| [Fe II], Fe II 4491 | | 0.6 | 0.8 | | 0.6 | [Fe VII], [Ca V] 6086 | 86.0 | | | | |
| He II 4541 | 1.1 | | | | | Fe II 6149 | | | 0.8 | 2.9 | 3.4 |
| Fe II 4584 | | | 1.3 | | 2.8 | Fe II 6240 | | | 0.7 | 5.5 | 3.8 |
| [Fe III] 4607 | 0.6 | | | | | Fe II 6248 | | | 0.8 | 3.5 | 2.9 |
| N III 4634 | 1.7 | | | | | [O I] 6300 | 31.8 | 29.0 | 25.1 | 16.9 | 13.0 |
| N III 4641 | 4.0 | | 1.1 | | | [S III] 6310 | 29.0 | | | | |
| [Fe III] 4658 | 3.0 | 1.1 | 0.8 | | | [O I] 6364 | 11.8 | 10.1 | 8.2 | 3.9 | 4.1 |
| He II 4686 | 39.1 | 1.1 | 1.1 | | | Fe II 6433 | | | 1.0 | 7.1 | 6.3 |
| [Fe III] 4702 | 2.2 | | 0.2 | | | [Ar V] 6435 | 7.5 | | | | |
| [Ne IV], He I 4714 | 3.8 | | 0.5 | | | Fe II 6456 | | | 1.2 | 4.4 | 4.8 |
| [Ne IV] 4725 | 4.7 | | 0.9 | | | Fe II 6516 | | | 1.4 | 5.3 | 7.1 |
| [Fe II] 4815 | 0.6 | 0.7 | 0.7 | | 1.1 | [N II] 6548 | | 28.1 | 20.6 | 30.0 | |
| H$\beta$ 4861 | 110.1 | 19.2 | 18.8 | 29.0 | 20.0 | H$_\alpha$ 6563 | 1790.0 | 173.6 | 145.8 | 700.0 | 630.0 |
| [Fe II] 4890 | 0.8 | 0.5 | 1.0 | 0.8 | 0.6 | [N II] 6584 | 79.1 | 78.2 | 64.4 | 60.0 | 53.4 |
| [Fe VII] 4894 | 1.1 | | | | | He I 6678 | 18.6 | 2.2 | 2.0 | | 1.0 |
| [Fe II] 4905 | 1.7 | | | 0.5 | 0.4 | [S II] 6717 | 3.8 | 2.8 | 2.2 | 1.1 | |
| He I 4922 | 2.0 | | | | | [S II] 6731 | 5.8 | 5.7 | 4.5 | 2.7 | |
| Fe II 4924 | | 1.5 | 1.6 | 4.0 | 5.5 | [Fe IV], [K IV] 6793 | 2.1 | | | | |
| [Fe VII] 4942 | 3.8 | | | | | He II 6891 | 2.4 | | | | |
| [O III] 4959 | 86.9 | 13.0 | 7.2 | | | [Fe IV] 6997 | 3.6 | | | | |
| [Fe VI] 4967 | 3.8 | | | | | [Ar V] 7006 | 23.2 | | | | |
| [Fe VI] 4973 | 4.0 | | | | | He I 7065 | 71.1 | 3.9 | | | |
| [Fe VII] 4989 | 1.9 | | | | | [Ar III] 7136 | 81.8 | | | 0.6 | |
| [Fe II] 5006 | | | | 1.1 | 0.9 | [Fe II] 7155 | 27.5 | | | 5.2 | 2.2 |
| [O III] 5007 | 263.7 | 44.1 | 23.3 | 3.9 | 1.1 | [Ar IV] 7170 | 2.0 | | | | |
| He I 5016 | 1.6 | | | | | [Fe II] 7172 | 18.2 | | | 1.3 | 1.9 |
| Fe II 5018 | | | 2.8 | 7.2 | 6.0 | He II 7177 | 5.4 | | | | |
| [Fe II] 5112 | | | 0.5 | 1.1 | 0.6 | O III 7189 | 1.8 | | | | |
| [Fe II] 5159 | | | 3.1 | 2.4 | 2.9 | [Fe IV] 7190 | 3.0 | | | | |
| Fe II 5169 | | | 2.3 | 7.8 | 9.0 | [Ca II] 7292 | | | | 21.5 | 23.2 |
| Fe II, [N I] 5198 | | | 1.3 | 2.1 | 2.0 | [O II] 7321 | | | | 3.8 | 5.2 |
| Fe II 5235 | | | 0.9 | 2.2 | 1.9 | [Ca II] 7324 | | | | 16.7 | 17.6 |
| Fe II 5285 | | | 0.6 | 2.0 | 2.8 | [O II] 7331 | | | | 3.4 | |

here (Table 4) might be slightly different from those published as they have been revised following the work by Carter (1990). The uncertainty on individual measurements is less than 0.03 mag in *JHK*, and less than 0.05 mag at *L*. Less precise observations are marked with a colon.

When available, the FES counts were converted to *V* magnitudes using the time-dependent correction from Fireman & Imhoff (1989) and the colour-dependent equations from Imhoff & Wasatonic (1986). The resulting magnitudes given in Table 1 have accuracies of 0.1 mag. We have also collected all published optical photometric data (Eggen 1973; Feast et al. 1977; Klutz 1979; W83; W84; Munari et al. 1992; IS94) as well as visual magnitude estimates reported on a regular basis by the Variable Star Section of the Royal Astronomical Society of New Zealand (RASNZ). Fig. 4 illustrates the $V/m_{\rm vis}$ light curve together with the infrared (IR) data.

## 3 ANALYSIS

### 3.1 Variability

#### *3.1.1 A brief survey of observations prior to 1969*

Although the first observational records of RX Pup date back to the end of the 19th century, the star has been generally neglected by most observers, and only sketchy information on its spectroscopic and photometric variations prior to the early 1970s is available.

RX Pup was classed among 'stars having peculiar spectra' by Fleming (1912). The spectrum taken on 1894 November 24 resembled that of $\eta$ Car, showing bright H$\beta$, H$\gamma$, H$\delta$ and H$\zeta$ (Pickering 1897). Another spectrum taken on 1897 January 8 showed, in addition to the strong H Balmer lines, bright He II $\lambda$4686, [O III] $\lambda$4363 and [Ne III] $\lambda$3869 (Cannon 1916). Cannon also noted that the spectral lines (although not their widths)

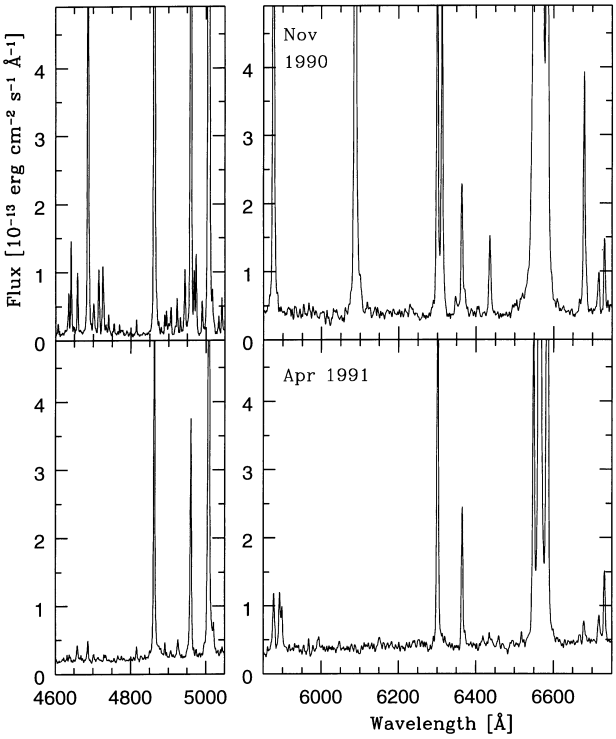


**Figure 3.** Optical spectra of RX Pup.

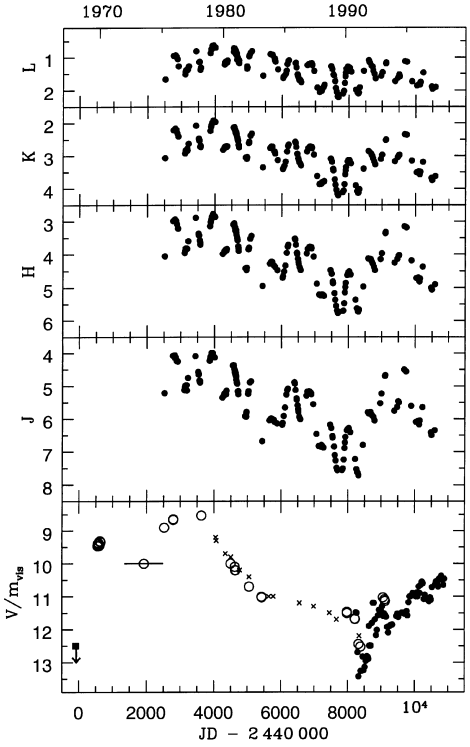


**Figure 4.** Optical and IR light curves of RX Pup in 1968–1998. Dots: visual observations from RASNZ; open circles: published *V* magnitudes; crosses: FES magnitudes; square with a down arrow: February 1968 visual mag limit.

resembled those of novae in the nebular phase. Extensive photometry obtained in 1890–1924 (Pickering 1914; Yamamoto 1924) showed the star brightened from $m_{pg} = 12$ in 1890 to $m_{pg} = 11.13$ in 1894, then declined to a very deep minimum ($m_{pg} = 14.1$) in 1904–5. After recovery c. 1909, the photographic magnitude showed only small fluctuations between 11.6 and 12.3 mag.

The next spectra of RX Pup, obtained in 1941 January, revealed a continuum confined to the yellow and red region, and very strong high-excitation emission lines of [Fe VII], [Ne V], [Fe VI] and [Ca VII], in addition to strong H I Balmer series, He II, [Ne III] and [O III] emission lines (Swings & Struve 1941). Swings & Struve also pointed out the spectroscopic similarity of RX Pup to the symbiotic stars CI Cyg and AX Per, although they did not find definite evidence for a late-type component in RX Pup.

The spectra taken between 1949 and 1951 showed very faint (or absent) continuum, moderately sharp H$\alpha$, as well as [O I] $\lambda\lambda$6300, 6364 and other blended emissions (most of them probably Fe II lines) between $\lambda$ 6300 Å and H$\alpha$ (Henize 1976). A similar low-ionization spectrum, with no He II $\lambda$4686, [O III] $\lambda$5007 very weak relative to H$\beta$ and a very faint continuum, was observed on 1968 February 26 by Sanduleak & Stevenson (1973) who also estimated the visual and photographic magnitudes at $m_{vis} \gtrsim 12.5$ and $m_{pg} = 13.5 \pm 0.5$, respectively.

### *3.1.2 The spectral transformations in 1969–1996*

Between 1968 and 1969 the optical brightness of RX Pup increased by a few magnitudes (Fig. 4). Between 1969 December and 1970 February, the star reached $V \sim 9.5$–9.3 (Eggen 1973). Its colours $B - V \sim 1.3$–1.2, $U - B \sim 0.5$–0.4, and $R - I \sim 0.8$, corrected for a reasonable amount of interstellar reddening, $E(B - V) \sim 0.6$ (Section 3.2), indicated the presence of a bright blue continuum. Optical spectroscopy obtained in 1972 February and 1975 March (Swings & Klutz 1976; also Webster & Allen 1975) revealed a bright late A- or early F-type continuum with strong H I as well as O I, [O I], Ca II, [Ca II] and numerous Fe II and [Fe II] emission lines. RX Pup maintained this low-excitation emission spectrum together with a strong blue continuum until 1979 March (Klutz, Simonetto & Swings 1978; Klutz & Swings 1981). The optical brightness reached a maximum in 1977–78, with $V \sim 8.5$, $B - V \sim 0.9$ and $U - B \sim 0.1 - 0.5$, and the optical spectrum resembled that of a Be or shell star (Feast et al. 1977; Klutz 1979). The first *IUE* spectrum taken in 1978 September (Fig. 1) shows a UV continuum like that of a Be/shell star. Similar optical/UV spectra have been observed in CH Cyg and other symbiotic stars during the visual maximum of their outbursts (Mikołajewska, Selvelli & Hack 1988; Kenyon 1986).

The H I Balmer lines presented double P Cygni profiles ($V << R$) in 1972, which evolved into a complex P Cygni structure in 1975, with one emission and a series of absorption components ranging from –1100 to –230 km s$^{-1}$ (Swings & Klutz 1976). Such complex structure was also observed in 1976, although higher members (such as H$\gamma$ and H$\delta$) showed very little absorption. In 1978 the Balmer lines became fairly stable emission lines with a sharp P Cygni profiles and a few fainter absorptions with positive velocities (Klutz 1979).

In December 1979 RX Pup returned to the high-excitation conditions exhibited 40 yr earlier; the appearance of strong and broad emission lines of He II, N III and [O III] in the optical range was accompanied by decline in the *UBV* fluxes (Klutz & Swings 1981; see Fig. 4). The Balmer continuum strengthened, and the intensities of the $\lambda$4640 feature and He II $\lambda$4686 emission resembled those observed in WN7–8 stars. The 1979 spectrum, however, showed neither [Fe VI] nor [Fe VII]. The next optical spectrum taken in 1983 April revealed faint [Fe VI] and [Fe VII] emission lines (W83), with a flux ratio [Fe VII] $\lambda$6086/He I $\lambda$5876 ~0.2. The

**Table 4.** Infrared photometry of RX Pup.

| JD 24... | J | H | K | L | JD 24... | J | H | K | L | JD 24... | J | H | K | L |
|---|---|---|---|---|---|---|---|---|---|---|---|---|---|---|
| 42520.50 | 5.21 | 4.05 | 3.06 | 1.67 | 44635.36 | 4.62 | 3.26 | 2.29 | 0.92 | 47124.56 | 6.83 | 5.21 | 3.86 | 2.06 |
| 42767.50 | 4.08 | 2.98 | 2.21 | 0.95 | 44639.36 | 4.68 | 3.31 | 2.34 | 0.92 | 47170.48 | 6.83 | 5.24 | 3.86 | 2.02 |
| 42795.50 | 4.09 | 2.95 | 2.19 | 0.95 | 44644.43 | 4.69 | 3.34 | 2.35 | 0.88 | 47188.47 | 6.85 | 5.24 | 3.85 | 2.02 |
| 42818.50 | 4.06 | 2.93 | 2.16 | 0.97 | 44647.38 | 4.71 | 3.35 | 2.35 | 0.95 | 47204.41 | 6.80 | 5.21 | 3.80 | 1.96 |
| 42820.50 | 4.08 | 2.96 | 2.19 | 0.93: | 44650.38 | 4.81: | 3.41 | 2.40 | 1.07 | 47238.33 | 6.84 | 5.22 | 3.79 | 1.91 |
| 42831.50 | 4.15 | 2.95 | 2.19 | 0.98 | 44668.35 | 4.86 | 3.48 | 2.44 | 1.01 | 47267.31 | 6.88 | 5.25 | 3.78 | 1.84 |
| 42851.50 | 4.13 | 2.98 | 2.20 | 0.98 | 44671.35 | 4.91 | 3.50 | 2.47 | 1.02 | 47464.61 | 6.18 | 4.48 | 3.09 | 1.28 |
| 42881.50 | 4.24 | 3.09 | 2.31 | 1.05 | 44683.32 | 4.93 | 3.57 | 2.53 | 1.06 | 47497.57 | 6.28 | 4.59 | 3.19 | 1.37 |
| 42911.50 | 4.25 | 3.21 | 2.40 | 1.27: | 44703.27 | 5.16 | 3.75 | 2.66 | 1.17 | 47533.52 | 6.53 | 4.82 | 3.40 | 1.53 |
| 43109.50 | 5.12 | 3.95 | 2.92 | 1.52 | 44712.24 | 5.15 | 3.81 | 2.68 | 1.09 | 47541.41 | 6.57 | 4.87 | 3.45 | 1.55 |
| 43121.50 | 5.04 | 3.88 | 2.89 | 1.43 | 44716.23 | 5.25 | 3.89 | 2.73 | 1.18 | 47583.38 | 6.84 | 5.17 | 3.72 | 1.73 |
| 43136.50 | 4.98 | 3.81 | 2.81 | 1.38 | 44918.60 | 5.92: | 4.42: | 3.05: | | 47607.36 | 7.10 | 5.37 | 3.89 | 1.94 |
| 43154.43 | 5.00 | 3.83 | 2.82 | 1.38 | 44948.59 | 5.90 | 4.41 | 3.06 | 1.28 | 47634.29 | 7.27 | 5.56 | 4.05 | 2.05 |
| 43174.48 | 4.97 | 3.81 | 2.77 | 1.37 | 44949.52 | 5.91 | 4.46 | 3.09 | 1.34 | 47661.26 | 7.49 | 5.70 | 4.16 | 2.19 |
| 43182.39 | 5.13 | 3.82 | 2.83 | 1.38 | 44950.56 | 5.93 | 4.47 | 3.09 | 1.35 | 47687.21 | 7.56 | 5.78 | 4.21 | 2.22 |
| 43215.32 | 4.75 | 3.59 | 2.62 | 1.27 | 44955.55 | 5.82 | 4.41 | 3.05 | 1.31 | 47823.61 | 7.56 | 5.72 | 4.11 | 2.10 |
| 43434.60 | 4.09 | 2.88 | 2.07 | 0.81 | 44960.50 | 5.79 | 4.41 | 3.04 | 1.31 | 47850.53 | 7.51 | 5.70 | 4.06 | 2.02 |
| 43519.50 | 4.57 | 3.36 | 2.46 | 1.14 | 45010.46 | 5.24 | 3.84 | 2.61 | 0.97 | 47873.53 | 7.24 | 5.48 | 3.87 | 1.79 |
| 43530.50 | 4.61 | 3.40 | 2.50 | 1.14 | 45017.40 | 5.18 | 3.80 | 2.57 | 0.94 | 47894.54 | 6.89 | 5.15 | 3.57 | 1.59 |
| 43532.48 | 4.65 | 3.42 | 2.53 | 1.13 | 45022.38 | 5.16 | 3.79 | 2.58 | 0.94 | 47907.47 | 6.72 | 4.99 | 3.45 | 1.48 |
| 43556.47 | 4.83 | 3.57 | 2.71 | 1.38 | 45060.29 | 4.89 | 3.52 | 2.38 | 0.85 | 47920.46 | 6.55 | 4.86 | 3.34 | 1.36 |
| 43572. | 4.88 | 3.70 | 2.72 | 1.33 | 45095.20 | 4.86 | 3.43 | 2.32 | 0.81 | 47964.35 | 6.35 | 4.63 | 3.18 | 1.29 |
| 43572.34 | 4.85 | 3.64 | 2.68 | 1.33 | 45432.25 | 6.68 | 4.95 | 3.35 | 1.56 | 47989.28 | 6.31 | 4.56 | 3.13 | 1.31 |
| 43573. | 4.89 | 3.69 | 2.71 | 1.31 | 45648.60 | 6.05 | 4.28 | 2.76 | 0.91 | 48022.33 | 6.29 | 4.52 | 3.14 | 1.33 |
| 43573.35 | 4.87 | 3.64 | 2.69 | 1.32 | 45687.46 | 5.99 | 4.22 | 2.71 | 0.93 | 48068.19 | 6.41 | 4.61 | 3.23 | 1.45 |
| 43860.56 | 4.23 | 3.14 | 2.23 | 0.87 | 45713.34 | 6.00 | 4.23 | 2.72 | 0.93 | 48213.52 | 7.22 | 5.37 | 3.90 | 1.99 |
| 43878.54 | 4.15 | 3.02 | 2.11 | 0.75 | 45773. | 6.06 | 4.34 | 2.86 | 1.03 | 48256.56 | 7.53 | 5.63 | 4.08 | 2.07 |
| 43881.47 | 4.10 | 3.00 | 2.11 | 0.76 | 45778. | 6.03 | 4.35 | 2.87 | 1.10 | 48281.44 | 7.62 | 5.72 | 4.13 | 2.10 |
| 43890.52 | 4.10 | 2.95 | 2.06 | 0.76 | 45800. | 6.09 | 4.38 | 2.93 | 1.14 | 48296.41 | 7.64 | 5.74 | 4.12 | 2.07 |
| 43896.46 | 4.09 | 2.93 | 2.05 | 0.73 | 45874. | 6.14 | 4.48 | 3.13 | 1.37 | 48321.40 | 7.71 | 5.67 | 4.02 | 1.92 |
| 43918.44 | 3.99 | 2.84 | 1.97 | 0.64 | 46029.50 | 6.19 | 4.70 | 3.41 | 1.63 | 48446.19 | 6.79 | 4.97 | 3.40 | 1.42 |
| 43922.43 | 4.03 | 2.85 | 1.97 | 0.68 | 46042.55 | 6.13 | 4.65 | 3.38 | 1.60 | 48593.60 | 5.80 | 4.13 | 2.85 | 1.09 |
| 43947.32 | 4.00 | 2.77 | 1.92 | 0.67 | 46074.50 | 5.92 | 4.52 | 3.30 | 1.56 | 48616.53 | 5.84 | 4.14 | 2.88 | 1.17 |
| 43949.33 | 4.00 | 2.78 | 1.91 | 0.63 | 46110.37 | 5.66 | 4.34 | 3.18 | 1.50 | 48670.48 | 5.80 | 4.15 | 2.94 | 1.26 |
| 43952.31 | 4.04 | 2.82 | 1.95 | 0.66 | 46133.39 | | | | 1.41 | 48700.37 | 5.86 | 4.23 | 3.00 | 1.29 |
| 44001.23 | 4.12 | 2.84 | 1.95 | 0.70 | 46153.32 | 5.26 | 3.95 | 2.87 | 1.21 | 48725.24 | 5.91 | 4.29 | 3.09 | 1.42 |
| 44008.23 | 4.13 | 2.86 | 1.96 | 0.70 | 46181.27 | 5.13 | 3.76 | 2.70 | 1.12 | 48765.22 | 5.96 | 4.39 | 3.18 | 1.52 |
| 44240.51 | 5.35 | 3.98 | 2.81 | | 46199.24 | 5.08 | 3.71 | 2.66 | 1.09 | 48792.19 | 6.05 | 4.48 | 3.27 | 1.65 |
| 44282.40 | 5.29 | 3.93 | 2.76 | 1.22 | 46393.59 | 4.89 | 3.52 | 2.57 | 1.18 | 48961.52 | 5.53 | 4.15 | 3.10 | 1.57 |
| 44295.37 | 5.24 | 3.89 | 2.72 | 1.14 | 46407.60 | 4.93 | 3.55 | 2.61 | 1.17 | 49001.34 | 5.23 | 3.97 | 2.97 | 1.46 |
| 44308.37 | 5.22 | 3.88 | 2.72 | 1.14 | 46425.60 | 5.12 | 3.71 | 2.73 | 1.31 | 49106.23 | 4.70 | 3.36 | 2.52 | 1.19 |
| 44317.36 | 5.23 | 3.87 | 2.71 | 1.16 | 46458.46 | 5.38 | 3.95 | 2.94 | 1.52 | 49113.20 | 4.67 | 3.32 | 2.50 | 1.16 |
| 44327.29 | 5.21 | 3.87 | 2.70 | 1.16 | 46465.44 | 5.42 | 3.99 | 2.96 | 1.57 | 49381.47 | 5.76 | 4.26 | 3.17 | 1.73 |
| 44331.26 | 5.20 | 3.85 | 2.71 | 1.12 | 46488.46 | 5.59 | 4.14 | 3.08 | 1.63 | 49468.34 | 5.64 | 4.14 | 3.04 | 1.63 |
| 44353.24 | 5.25 | 3.88 | 2.72 | 1.16 | 46503.33 | 5.71 | 4.23 | 3.14 | 1.68 | 49503.25 | 5.47 | 4.04 | 2.98 | 1.53 |
| 44364.23 | 5.14 | 3.83 | 2.70 | 1.09 | 46514.32 | 5.79 | 4.30 | 3.19 | 1.70 | 49519.19 | 5.50 | 4.03 | 2.98 | 1.59 |
| 44551.61 | 4.38 | 3.09 | 2.13 | 0.83: | 46540.35 | 5.94 | 4.40 | 3.23 | 1.70 | 49676.53 | 4.50 | 3.15 | 2.34 | 1.12 |
| 44554.57 | 4.37 | 3.09 | 2.13 | 0.72 | 46569.21 | 6.01 | 4.48 | 3.30 | 1.76 | 49734.56 | 4.56 | 3.19 | 2.36 | 1.14 |
| 44578.58 | 4.37 | 3.05 | 2.12 | 0.73 | 46752.59 | 5.29 | 3.97 | 2.87 | 1.25 | 49887.22 | 5.61 | 4.19 | 3.15 | 1.74 |
| 44582.56 | 4.38 | 3.10 | 2.15 | 0.75 | 46783.50 | 5.17 | 3.83 | 2.77 | 1.22 | 50034.55 | 6.10 | 4.72 | 3.51 | 1.87 |
| 44593.52 | 4.48 | 3.17 | 2.21 | 0.78 | 46825.42 | 5.16 | 3.78 | 2.73 | 1.21 | 50089.50 | 6.07 | 4.70 | 3.48 | 1.83 |
| 44596.55 | 4.50 | 3.16 | 2.20 | 0.81 | 46833.43 | 5.19 | 3.79 | 2.75 | 1.22 | 50111.43 | 6.13 | 4.78 | 3.53 | 1.81 |
| 44606.54 | 4.51 | 3.18 | 2.23 | 0.79 | 46844.44 | 5.16 | 3.77 | 2.71 | 1.19 | 50123.49 | 6.18 | 4.82 | 3.57 | 1.84 |
| 44613.50 | 4.59 | 3.28 | 2.30 | 0.91 | 46881.33 | 5.20 | 3.77 | 2.73 | 1.18 | 50142.46 | 6.06 | 4.74 | 3.49 | 1.76 |
| 44614.54 | 4.54 | 3.23 | 2.25 | 0.87 | 46897.29 | 5.23 | 3.81 | 2.74 | 1.22 | 50221.28 | 5.65 | 4.38 | 3.19 | 1.47 |
| 44620.49 | 4.60 | 3.24 | 2.28 | 0.88 | 46897.33 | 5.25 | 3.82 | 2.77 | 1.25 | 50478.48 | 6.41 | 5.01 | 3.68 | 1.90 |
| 44627.41 | 4.65 | 3.26 | 2.33 | 0.89 | 46955.26 | 5.56 | 4.07 | 2.97 | 1.42 | 50498.45 | 6.50 | 5.07 | 3.75 | 1.96 |
| 44631.42 | 4.60 | 3.27 | 2.30 | 0.92 | 47055.65 | 6.46 | 4.89 | 3.62 | 1.93 | 50590.23 | 6.35 | 4.91 | 3.63 | 1.91 |

intensity of the [Fe VII] was growing, and in the 1984/89/90 spectra (AW88; de Freitas Pacheco & Costa 1992, hereafter FPC92; Table 3) the [Fe VII] λ6086/He I λ5876 flux ratio increased to 0.3/1.7/1.4, respectively. The changes in the optical spectrum observed between 1979 and 1989 clearly indicate a gradually increasing degree of ionization, similar to that reported for symbiotic novae (e.g. Kenyon 1986).

The evolution of the blue continuum and emission-line spectrum

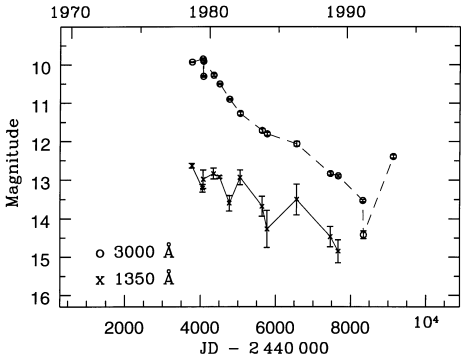


**Figure 5.** Variation of UV continuum magnitude in 1978–1993.

in 1978–1993 can be traced best using *IUE* data. Fig. 1 illustrates the changes in the UV. To establish the continuum behaviour, we measured average fluxes, $F_\lambda$, in 20-Å bins free from emission lines and derived magnitudes using $m_\lambda = -2.5 \log F_\lambda - 21.1$. The continuum declines steadily from 1978 to 1991, in a similar way to the visual light (Figs 5 and 4); the UV continuum seems to fade less at short wavelengths ($\lambda\lambda \lesssim 1500$ Å) than at longer wavelengths ($\lambda\lambda \lesssim 2500$ Å). The continuum decline is matched by an increase in flux from most of the emission lines (Fig. 6). In particular, the He II λ1640 flux increased by a factor of ∼5 between 1979 June and 1980 April. The He II flux continued a slower increase until 1981 June and from then to the observation of 1986 May it remained at a roughly constant level. Similar behaviour was seen amongst other medium-excitation lines, such as C IV λ1550, N IV] λ1487, Si IV λ1394 and O IV] λ1403. N V λ1240 appeared for first time in 1981 June, while [Mg V] λ2783 appeared in 1983 October (Fig. 7); these lines showed maximum fluxes in the spectra taken during 1986 and 1988, respectively. Generally, the trends observed in the UV

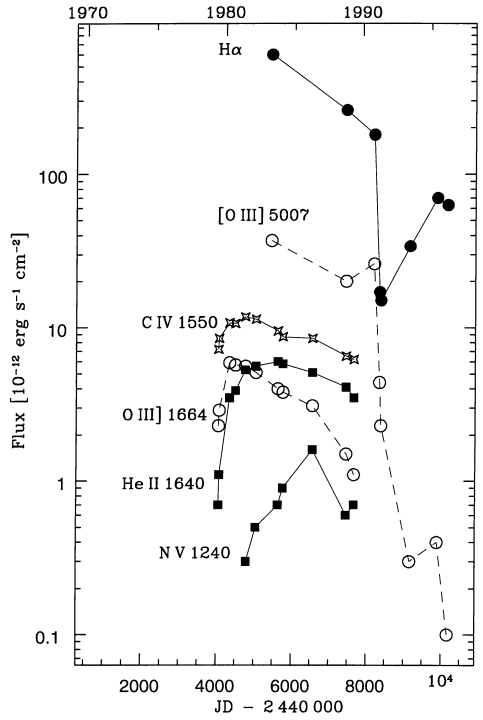


**Figure 6.** Evolution of optical and UV emission-line fluxes in 1979–1996. The Hα and [O III] λ5007 fluxes published by W83, van Winckel, Duerbeck & Schwarz (1993) and IS94 are also plotted.

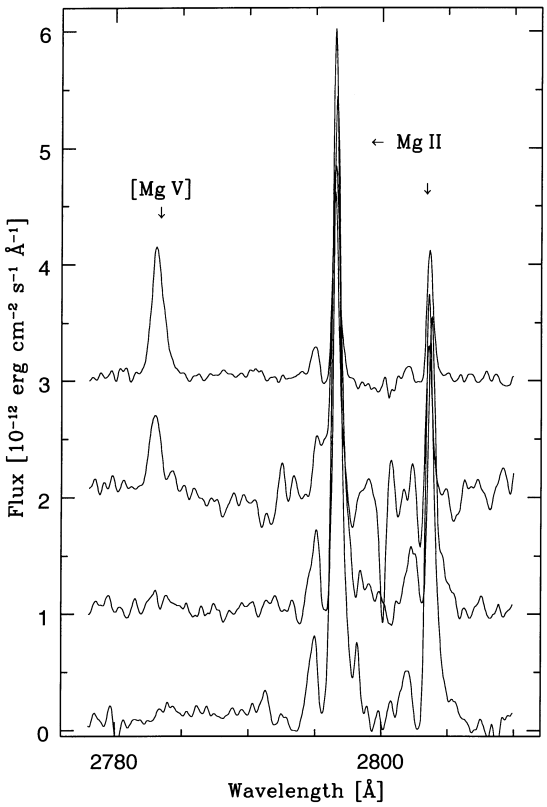


**Figure 7.** Appearance and evolution of [Mg V]. The high-resolution spectra, which were taken on (from bottom to top) 1982 March 22, 1983 October 30, 1986 May 9 and 1988 October 25, respectively, show the appearance and increase of [Mg V] λ2783.

continuum and emission-line fluxes show an evolution towards higher stages of ionization, similar to that observed in symbiotic novae (Nussbaumer & Vogel 1990; Mürset & Nussbaumer 1994).

From an analysis of high-resolution *IUE* spectra taken between 1980 September and 1984 March, K85 (also K82) found that many of the strong emission lines exhibit multiple component structure. Our analysis, however, does not confirm some of their identifications. For example, the redshifted component of He II λ1640 as well as the blueshifted component of N III] λ1749.7 (figs 1b and 1d of K85) are misidentified as O I] λ1641.4 and N III] λ1748.6, respectively. The intensity of the λ1641 feature is strongly correlated with the O I λ1304 line flux measured on low-resolution spectra; this feature is absent on all high-resolution spectra taken in 1983–1988 when the O I λ1304 was very faint or absent. Moreover, profiles of all semiforbidden emission lines detected on the high-resolution spectra show more or less the same velocity structure, with a width at the foot of $\sim 250\,\mathrm{km\,s^{-1}}$ centred roughly at the stellar velocity ($\sim 10\,\mathrm{km\,s^{-1}}$; Wallerstein 1986). The only exception would be N III] λ1749.7 if the K85 interpretation were accepted. We also disagree with K85 about the close similarity between the C IV and He II profiles. The C IV λλ1548.2, 1550.8 doublet emission profile is truncated by a narrow P Cygni structure at $\sim -90\,\mathrm{km\,s^{-1}}$, and it exhibits rather complex structure, while He II has a considerably simpler profile which is almost symmetric around the stellar velocity.

The C IV doublet shows unusual intensities: the $I(\lambda 1548.2)/I(\lambda 1550.8)$ ratio had an observed value of ∼0.6 in 1980–82, then in 1983 its value increased to ∼0.8. In 1987 the C IV doublet ratio reached the optical thick limit of unity (see also Michalitsianos et al.

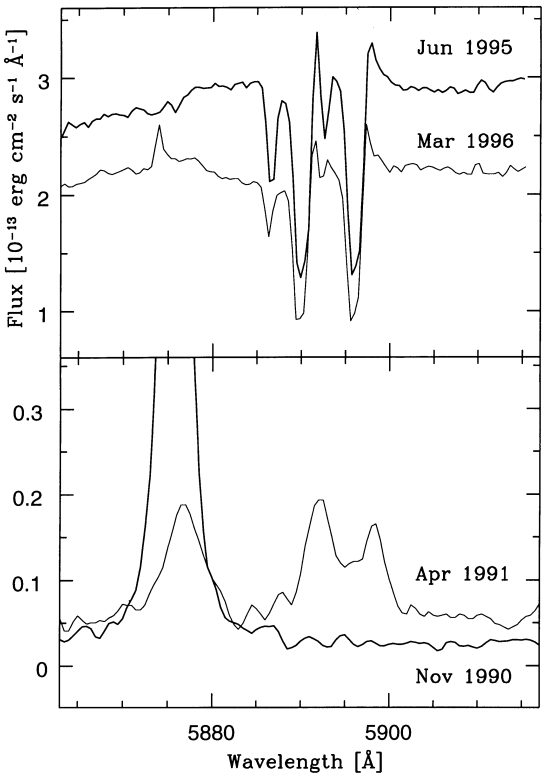


**Figure 8.** Evolution of Na I $D_1, D_2$ lines.

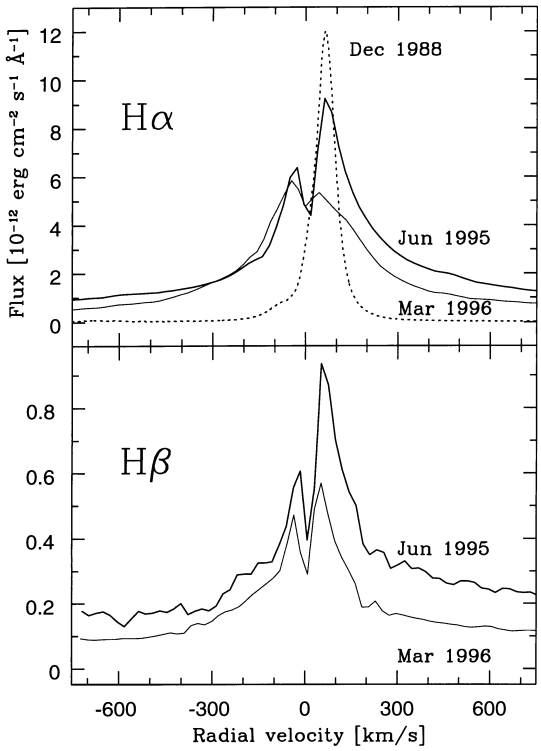


**Figure 9.** The H I Balmer lines in 1995 and 1996 (thick and thin line, respectively) exhibited strong central absorptions which were probably responsible for the very steep decrement. The H$\alpha$ profile (dotted line) observed in 1988 by van Winckel et al. (1993) is shown for comparison.

1988), while in 1988 $I(\lambda1548.2)/I(\lambda1550.8) \simeq 1.1$. The C IV ratio seems to increase following the general enhancement of high-excitation emission line fluxes (Table 2; Fig. 6). Similar behaviour was reported in the symbiotic nova HM Sge (Müller & Nussbaumer 1985). Michalitsianos, Kafatos & Meier (1992) demonstrated that the combined fluxes of Fe II Bowen-pumped lines can account for an appreciable portion of the flux deficit in the C IV λ1548.2 line in 1980–83, when the C IV doublet ratio is less than the optically thick limit. Their interpretation is consistent with the presence of O I] λ1641.3 in 1980–83, indicating the emitting region was optically thick.

By early 1991, the high-excitation emission lines had practically disappeared. The *HST* spectrum taken in 1991 March (Fig. 3) revealed a very faint UV continuum without strong emission lines. In particular, the intercombination Si III] λ1892 and C III] λ1909, still strong on the SWP spectrum of 1989 May, had disappeared, as had the O III λ3133 emission, which was very strong in the 1980s. The only emission detected in the UV range was a weak Mg II λ2800. The optical continuum was also faint, consistent with the deep minimum shown by the $V/m_{\rm vis}$ light curve at this time (Fig. 4). The lack of measurable short-wavelength continuum or emission lines (except Mg II λ2800 and very faint Fe II λ2756) was confirmed by the *IUE* spectra taken a few days after the *HST* data. The optical spectra taken in 1991 April and May also showed a significant decline in the continuum and emission-line fluxes (Fig. 3 and Fig. 6). The only emission lines that remained practically unchanged were low-excitation forbidden lines [O I], [N II] and [Fe II]. The 1991 spectrum was also characterized by the appearance of Na I D in emission (Fig. 8). The decrease in the He II/H$\beta$ ratio from ~0.4 in the 1990s to ~0.06 in 1991 suggests a general decline of the source of ionization.

Between 1992 and 1993, the optical magnitudes recovered to about the same level as in the late 1980s (Fig. 4); the degree of excitation, however, continued to decrease. He II λ4686 was absent on optical spectra taken in 1995 and 1996, and the fluxes in practically all of the emission lines were significantly reduced. The only lines that remained relatively strong were the Balmer H I lines (H$\alpha$ brightened by a factor of ~4 since 1991; Fig. 6), although weak low-excitation lines from Fe II and forbidden transitions were also visible. The Balmer decrement was unusually steep, H$\alpha$:H$\beta \sim 30$, and both H$\alpha$ and H$\beta$ had deep central absorptions (Fig. 9).

RX Pup also exhibits interesting variability at radio wavelengths. In the mid-1970s, when detected for the first time, the radio emission was characterized by a flat, optically thin spectrum. By 1985 it had changed to a steeply rising spectrum (Seaquist & Taylor 1987). In the 1990s, it flattened at all wavelengths with the previous level of flux density maintained only at the longest wavelength (IS94). The transition from a steep to a flat radio spectrum seems to have occurred between 1991 February and December (IS94). The 3.5-cm flux dropped from $S_{8.3\rm GHz} = 69.7 \pm 3.5$ mJy in 1991 February (Seaquist, Krogulec & Taylor 1993) to $S_{8.9\rm GHz} = 11.3 \pm 0.3$ mJy in 1992 July (ATCA; Lim, private communication) and was apparently related to changes in the UV and optical spectra.

In contrast to the optical brightness, the infrared *JHKL* light curves are dominated by periodic variations consistent with those expected for a Mira variable, and a long-term, wavelength-dependent, decrease of the mean brightness (Fig. 4). A Fourier analysis of the data in Table 4 confirms the pulsation period of 578 d found by Feast et al. (1977). The following ephemeris gives the phases of minima in the *J* band:

$$\min(J) = 244\,0214 + 578 \times E. \quad (1)$$

The long-term trends were attributed to dust obscuration possibly

related to the orbital motion (W84; Whitelock 1987). The IR fading is strongest in the $J$ band, and decreases in amplitude with increasing wavelength. We estimate the mean fading rates in 1979–1991, $\Delta J \sim 0.2$, $\Delta H \sim 0.12$ and $\Delta K \sim 0.08$ mag yr$^{-1}$, respectively. The fading started in late 1979, following the decline in visual brightness and appearance of the high-excitation emission-line spectrum. The faintest infrared flux was measured around 1991, after which the *JHKL* magnitudes recovered to the values observed in 1982–1983.

Several authors claimed that the visibility of molecular bands from the Mira component of RX Pup is limited to the periods of low excitation (IS94, and references therein). In fact, although RX Pup was undoubtedly in the low-excitation phase in the 1970s, red and blue spectra taken in 1972 show no trace of absorption bands (Swings & Klutz 1976). Similarly, Swings & Klutz failed to detect any TiO bands at $\lambda \lesssim 8600$ Å on their spectra taken in 1975 March. Strong TiO bands in the λλ7589–8432 range as well as VO λ7900 were detected, for the first time, on 1980 November 30 (Andrillat 1982), after RX Pup entered a high-excitation phase (!). Although Schulte-Ladbeck (1988) did not find any TiO at $\lambda \lesssim 8000$ Å, the TiO as well as VO bands were visible beyond $\lambda \sim 8000$ Å in 1984 April (AW88). Similarly, there were no detectable absorption bands in our red spectra taken in 1990 and 1991 ($\lambda \lesssim 7200$ Å), while the absorption bands beyond $\lambda \sim 7200$ Å were present in spectra taken in 1993 by IS94, and in our spectra taken in 1995 and 1996. In all cases, the absorption bands of the Mira variable were detected beyond $\lambda \sim 7000$ Å. In particular, the TiO bands at λ6180 and λ7100 Å, strong in most symbiotic systems (Kenyon & Fernandez-Castro 1987), were never detected in RX Pup, including our well-exposed spectra of 1995 and 1996. The only positive detections were made in the long-wavelength range, $\lambda \gtrsim 7200$ Å, when the visual magnitude of RX Pup was $V \sim m_{\rm vis} \gtrsim 10.5$ and near maxima of the pulsations of the Mira variable. The permanent absence of the molecular absorption bands in the optical range is consistent with the fact that the Mira pulsations were never visible in that range (Fig. 4). Similar behaviour is shown by other symbiotic Mira variables. In particular, Mira pulsations were never observed in the optical light of HM Sge, even during quiescence (Yudin et al. 1994).

The evolution of the $B-V$ and $U-B$ colour indexes in RX Pup also suggests that the contribution of the Mira to the optical light was never significant. The $B-V$ index had roughly constant value ∼0.9 in 1975–1990, which increased to ∼1.7 in 1993, while the $U-B$ index increased from ∼0.1 in 1975 to ∼0.5 in 1979, then decreased to $\sim -0.5$ in 1989–1990, and increased again to $\sim 0.4-0.5$ in 1993 (Feast et al. 1977; Klutz 1979; Munari et al. 1992; IS94). AW88 found that the 1984 optical continuum resembled reddened gaseous emission. We estimate the contribution of the emission lines to the observed broad-band $B$ and $V$ magnitudes as $\Delta V \sim 1/0.25/0.05$ and $\Delta B \sim 1.8/0.45/0.05$ mag in 1990/91/95, respectively. During the 1993 observation the Mira component was near maximum of its pulsation variability ($\phi \sim 0.9$). Given the reddening towards RX Pup, $E(B-V) \gtrsim 0.6$ (Section 3.2), and that near maximum light long-period Mira variables have $B-V \sim 1.6$ and $U-B \sim 1$ (Smak 1964), the observed values of $U-B$ and $B-V$ for RX Pup are similar to those found in other symbiotic systems, and indicate the hot component dominates at these wavelengths.

Fig. 10 summarizes the spectral development of RX Pup during the last three decades. The parallel between RX Pup and the symbiotic novae AG Peg (Gallagher et al. 1979; Kenyon et al. 1993), V1329 Cyg (Kenyon 1986, and references therein) and HM Sge (Nussbaumer & Vogel 1990) as well as the symbiotic recurrent nova RS Oph (Kenyon 1986) is apparent, although these other systems seem to be evolving on very different time-scales.

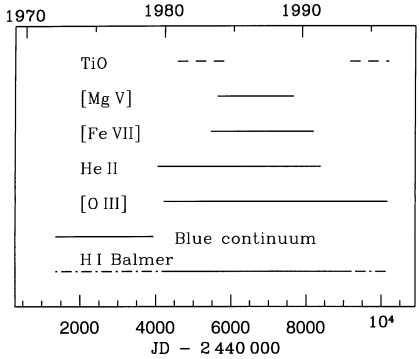


**Figure 10.** Spectral development of the 1969–1990 outburst of RX Pup. Solid, dashed and dot–dashed lines indicate emission and absorption features, and complex P Cyg profiles, respectively.

### 3.2 Reddening and distance

Before deriving the physical characteristics of the RX Pup binary, we need a good estimate for the extinction and distance. We base our reddening estimates on the UV continuum, UV and optical emission-line ratios, IR photometry and measurements of the interstellar features. We also assume the reddening to be represented by a standard interstellar extinction curve (e.g. Seaton 1979).

#### *3.2.1 Interstellar absorption features*

RX Pup lies in field 99(256/–3.0) of Neckel & Klare (1980), for which they estimate the interstellar reddening to be $E(B-V) \sim 0.6$ at $d \sim 1.3$–2 kpc. For such an $E(B-V)$ we would expect measurable interstellar features.

In fact, Klutz et al. (1978) reported interstellar Na I $D_1, D_2$ absorption lines as well as broad absorption bands at $\lambda \sim 5780$ and 5797 Å. The total equivalent width, EW($D_1 + D_2$) ∼ 0.43 Å, measured by Klutz et al. implies $E(B-V) \lesssim 0.1$ (Sembach, Danks & Savage 1993; Munari & Zwitter 1997), while EW(λ 5780) = 0.45 Å and EW(λ 5797) = 0.52 Å combined with the calibrations of Josafatsson & Snow (1987) and Herbig (1993) indicate a much higher $E(B-V) \sim 0.8$–1.0. The latter value is comparable to our estimates based on emission-line ratios (see below), but higher than the interstellar reddening predicted by Neckel & Klare (1980).

The absorption lines of Na I $D_1, D_2$ are also clearly visible in our optical spectra taken in 1995 and 1996 (Fig. 8). The profiles are, however, very complex, with faint emission features truncated by very strong absorption components, EW($D_1$) ∼ EW($D_2$) ∼ 1 Å, at $\sim -2$ km s$^{-1}$, and weaker components, EW($D_1$) ∼ 0.3–0.4 and EW($D_2$) ∼ 0.1 Å, at $\sim -180$ km s$^{-1}$, in both spectra. Traces of both absorption components are also visible in the emission-line profiles of Na I on the spectrum taken in 1991 April. The ESO spectrum (1991 May) has insufficient resolution to show them. In addition, the 1995 spectrum shows strong K I λλ 7665, 7699 absorption lines [EW(7665) ∼ 1.3 Å, EW(7699) ∼ 0.8 Å] at ∼1 km s$^{-1}$, very close to the radial velocity of the stronger components of the Na I D lines. It seems unlikely that these strong absorption features are of interstellar origin. The radial velocities of the K I absorption lines and of the stronger components of the Na I lines are $\sim -16$

and $-19$ km s$^{-1}$, respectively, with respect to the local standard of rest (LSR) and they are blueshifted with respect to the velocity predicted by galactic rotation law ($v \sim 5$–$10$ km s$^{-1}$ for a reasonable range $d \sim 1$–$2$ kpc). The K I line is somewhat asymmetric, while the Na I absorption lines seems to consist of two components. The strong absorption components of the Na I doublet as well as the K I absorption lines are probably superpositions of the interstellar and circumstellar/stellar components.

Adopting the calibration of Bromage & Nandy (1973), we estimate from the combined equivalent widths of both Na I D lines [EW($D_1 + D_2$) $\sim$ 2Å] $E(B-V) \gtrsim 0.6$. Other calibrations give similar results, for example Munari & Zwitter (1997) find EW($D_1$) $\sim$ 1 Å for $E(B-V) \gtrsim 0.5$ and stars with multicomponent interstellar lines. However, the K I absorption lines are too strong for any plausible $E(B-V)$ (e.g. Chaffee & White 1982; Munari & Zwitter 1997).

The spectra taken in 1995 and 1996 also show the diffuse interstellar bands at λ$\sim$ 5780, 5797 and 6284 Å. Their equivalent widths, EW(λ5780) $\approx$ 0.21 Å, EW(λ5797) $\approx$ 0.12 Å and EW(λ6284)$\approx$ 0.22 Å, are consistent with $E(B-V) \sim 0.5$ (Herbig 1993; Josafatsson & Snow 1987; Snow, York & Welty 1977).

### 3.2.2 *UV continuum*

An independent reddening estimate towards the hot component of RX Pup can be derived from the intensity of the λ2200 band. Unfortunately, practically all *IUE* spectra have very poorly exposed continua. The only spectra that can be used are SWP 2684 and LWR 2395, taken near the visual maximum in 1978. These show characteristic features of the iron curtain absorption and a strong absorption band around λ2200 Å. We compared the combined SWP + LWR spectrum with the *IUE* spectra of CH Cyg taken during its 1981–1984 visual maximum (Mikołajewska et al. 1988), and estimated $E(B-V) \lesssim 0.6$.

The very strong absorption feature near λ2200 Å is also visible on the *HST* spectrum taken in 1991 May. Correcting this spectrum for $E(B-V) \sim 0.8 \pm 0.1$ entirely removes the feature, and the dereddened spectrum resembles that of CH Cyg observed during the 1985 minimum (Mikołajewska et al. 1988). Given the uncertainty in the shape of the hot component UV continuum, these estimates generally agree with those derived from the emission lines.

### 3.2.3 *Emission lines*

Both the [Ne V] λλ 1575, 2975 lines originate from the same upper level, as do the [Fe VII] λλ 5721, 6086 lines. Thus their intensity ratio should depend only on the transition probabilities, [Ne V] $I(\lambda1575)/I(\lambda2975) = 1.5$ and [Fe VII] $I(\lambda5721)/I(\lambda6086) = 0.65$, respectively. The average [Ne V] ratio, $\sim$0.6 measured from the *IUE* spectra taken in 1983–1988, implies $E(B-V) = 0.4 \pm 0.4$. The high uncertainty is a result of the faintness of the [Ne V] lines. The [Fe VII] line ratio observed in 1983 by W84 indicates $E(B-V) = 1.4 \pm 0.5$, and data from FPC92 give $E(B-V) = 1.9 \pm 0.5$ in 1989. These values should, however, be considered as upper limits for $E(B-V)$ because the [Fe VII] λ6086 line can be strongly blended with the [Ca V] λ6086 line.

A better reddening estimate can be made from the [Ne IV] λ1602/λ4725 ratio (e.g. Schmid & Schild 1990a). The intensity of the ultraviolet [Ne IV] λ1602 emission line was almost constant in 1980–89. We compared its average flux with that in the optical [Ne IV] λ4725 line (W84), and estimate $E_{B-V} = 0.9 \pm 0.1$.

The [O II] $I(\lambda7325)/I(\lambda2471)$ ratio has an almost constant value of 1.27 for electron temperatures, $T_e$, between 5000 and 20 000 K and densities, $n_e$, from 10 to $10^6$ cm$^{-3}$ (Cantó et al. 1980). The λ 2471 line is absent in the *IUE* spectra taken before 1983, while very weak emission appears in later spectra. The optical [O II] λ7325 doublet was measured from our 1995 and 1996 spectra, and it seems to be also present in the 1993 spectrum (IS94). The λ 7325 emission was also present in the 1984 spectrum published by AW88, and the 1989 spectrum measured by FPC92. Our estimate of $I(\lambda7325)/I(\lambda2471) \gtrsim 40$ in 1984 and 1989 is consistent with $E(B-V) \gtrsim 0.7$. Similarly, $I(\lambda7325)/I(\lambda2471) \gtrsim 13$ in 1993–1996 suggests $E(B-V) \gtrsim 0.5$.

Extinction parameters can also be estimated from optical H I, He I and He II recombination lines. The ratios of He II λ1640, λ2733 and λ3203 lines observed in 1982–1988 are consistent with case B recombination and $E_{B-V} = 0.7 \pm 0.1$. The He II λ1640 emission-line flux was practically constant in 1982–1984. Combining the average flux in the UV line with that in He II λ4686 measured in 1983 by W84, we estimate $I(\lambda1640)/I(\lambda4686) \approx 0.3$ on JD 244 5459, which indicates $E(B-V) \approx 0.8$. Finally, the published He II λ4686/λ5411 ratios indicate $E(B-V) \sim 1.4$ (W84) and $\sim$1.2 (FPC92), respectively. These values should, however, be considered as upper limits because the λ5411 line is blended with Fe II λ5413 and [Fe IV] λ5426.

The H I Balmer lines are reliable reddening indicators only for negligible self-absorption in the lower series members (case B recombination, e.g. Cox & Mathews 1969; Netzer 1975). For most D-type symbiotic systems, reddening values estimated assuming case B recombination agree with those derived using other methods (Mikołajewska, Acker & Stenholm 1997). In the case of practically all S-type systems, and some D-types, there are significant departures from case B, and the reddening-free Hα/Hβ ratio is $\sim$5–10 (e.g. Mikołajewska & Kenyon 1992a; Mikołajewska et al. 1995; Proga et al. 1996; Mikołajewska et al. 1997) because of self-absorption. In particular, Hα/Hβ $\sim$ 5–10 is found at the high electron densities, $n_e \sim 10^9$–$10^{10}$ cm$^{-3}$ (Drake & Ulrich 1980) that characterize the Balmer line formation region (see Section 3.4).

The values of Hα/Hβ, Hγ/Hβ and Hδ/Hβ from W84 and FPC92 are inconsistent with case B recombination for any reddening. If the Hα optical depth is $\tau_{H\alpha} \sim 5$–$10$, the line ratios imply $E(B-V) \sim 1$. The H I ratios measured in 1991 (JD 244 8385; Table 3) are consistent with case B recombination, and $E(B-V) = 1.0 \pm 0.1$. Finally, our observations in 1995 and 1996 show a very steep Balmer decrement, Hα/Hβ = 24 and 31, respectively. Similarly, IS94 measured Hα/Hβ = 31 in 1993 June. IS94 also derived $E(B-V) \sim 0.4$, comparing the flux in Hβ with the radio flux at 5 GHz observed at the same epoch. However, their estimate assumes case B recombination, and is entirely inconsistent with the $E(B-V) \sim 2.3$ suggested by the Hα/Hβ ratio. The H I emission line profiles observed in 1995 and 1996 are complex with central reversals (see also Fig. 9). The Hα, Hβ and Hγ lines are apparently affected by self-absorption. The higher members are generally less affected. In particular, the Hγ/Hβ ratio differs from the case B value by less than 10 per cent as long as $\tau_{H\alpha} \lesssim 100$ (Netzer 1975; Proga et al. 1996). Assuming that the bulk of H I Balmer emission originates from the same region as the optical He I and UV intercombination lines, we estimate $\tau_{H\alpha} \lesssim 20$ in the 1980s and 1995–96, and $\lesssim$0.5 in 1991. The observed Hγ/Hβ ratio was practically constant in 1983–1996 within the observation accuracy of 5–10 per cent, and its mean value 0.32 ± 0.01 is consistent with $E(B-V) = 0.8 \pm 0.3$.

The calculations of Proga, Mikołajewska & Kenyon (1994) demonstrated that the He I $I(\lambda6678)/I(\lambda5876)$ emission-line ratio

distinguishes between S- and D-type systems in that it is ≈0.25 for D-types and ≳0.5 for S-types. The average He I $I(\lambda6678)/I(\lambda5876) = 0.38 \pm 0.03$ for RX Pup indicates $E(B-V) = 1.0 \pm 0.3$.

The emission-line ratios thus generally indicate a reddening of $E(B-V) \sim 0.8$ to 1.0 during the period 1980–1991.

### 3.2.4 *Mira component*

It is clear (see Section 3.1) that the Mira component made a negligible contribution to the optical light, at least during the last three decades. Therefore, estimates of the reddening toward the Mira component must be based on an analysis of the infrared. As the IR light curves (Fig. 4) show large variations in the average light and colour of the Mira component, we made independent estimates for four different epochs corresponding to different stages of the hot component (see also Section 3.3):

(i) epoch I: JD 244 2767–4000: the optical maximum and low-excitation phase;
(ii) epoch II: JD 244 5000–6600: constant hot component luminosity and high-excitation phase;
(iii) epoch III: JD 244 7500–8500: optical and IR minimum;
(iv) epoch IV: JD ≳ 244 8500: quiescence and low ionization.

The colours of Miras have been discussed by Feast et al. (1989) for the Large Magellanic Cloud, Whitelock et al. (1994) for the South Galactic Cap (SGC) and Glass et al. (1995) for the bulge.[1] These results suggest that the colours of Miras depend to some extent on the environment in which they occur, probably as a result of the different metallicities of the various environments. However, $(J-K)$ appears to be less sensitive to metallicity variations than are other colours. It also provides a longer baseline for reddening estimates than $(J-H)$ or $(H-K)$ and avoids any contribution from dust emission that may affect the $L$ observations. We therefore use $(J-K)$ in this analysis in preference to other IR colours.

The reddening towards the Mira component was estimated using the $(J-K)$ period–colour relation derived by Whitelock et al. (in preparation) for Miras in the solar neighbourhood:

$$(J-K)_0 = -0.78 + 0.87 \log P. \quad (2)$$

Thus for RX Pup, $(J-K)_0 = 1.63$. The values derived are listed in Table 5.

W83 suggested that there may have been a hot source contributing to the IR during what we are now calling epoch I. We also note that the Mira pulsation amplitude was low ($\Delta J \sim 1$, $\Delta K \sim 0.8$ in epoch I, and $\Delta J \sim 1.4$, $\Delta K \sim 1$ during remaining epochs) at this stage, consistent with the additional contribution from a warm non-pulsating source. We therefore deduce that during epoch I, the hot component contributed significantly to the $J$ flux. The value of $E(B-V)$ tabulated for this phase is therefore likely to be an underestimate. A similar effect may have been observed in HM Sge, where the amplitude of Mira pulsations decreased from $\Delta J \sim 1.2$ at the visual maximum during the hot component outburst to $\Delta J \sim 2$ mag during the late outburst decline.

Unfortunately, almost all well-studied long-period Miras ($P \gtrsim 400$ d) experience circumstellar reddening, although some have much more than others (e.g. Whitelock et al. 1994; Glass et al. 1995). Three Miras in the South Galactic Cap (SGC) have periods similar to RX Pup; they are AW Psc, AFGL 5592 and NSV 14540 (Whitelock et al. 1994). The colours of these stars [$(J-K)$ = 1.9 to 2.4] may be presumed to be unaffected by interstellar reddening. Thus, if we assume that interstellar (or interstellar plus circumbinary) reddening produces $E_{J-K} \sim 0.4$ (corresponding to $E(B-V) = 0.8$), it appears that the colours of RX Pup were quite normal during phases II and IV. During phase III, however, the Mira variable was considerably redder.

[1]Note that these papers present data on two different photometric systems, thus transformations must be made before stellar colours can be compared.

**Table 5.** Reddening towards the Mira component of RX Pup.

| Epoch | $\overline{K}$ | $\overline{J-K}$ (mag) | $E(B-V)$ |
|---|---|---|---|
| I | 2.37 | 2.13 | > 1.0 |
| II | 2.90 | 2.72 | 2.3 |
| III | 3.68 | 3.24 | 3.3 |
| IV | 3.12 | 2.58 | 2.0 |

We also find that the IR continuum energy distribution of RX Pup observed by *IRAS* (during epoch II) is practically identical to the IR continua of the long-period SGC Miras (AW Psc, AFGL 5592 and NSV 14540) mentioned above. This supports the interpretation that, during phases II and IV, the Mira in RX Pup was a normal high mass-loss AGB star. Whitelock et al. (1994) also show correlations between mass-loss rates and $K-[12]$ colour, pulsation period, and the amplitude of the $K$-light curve for their SGC sample. The observed $K-[12] \approx 4.6$ (the $K$ magnitude has been corrected for $E(B-V) \sim 1$) for RX Pup implies $\dot{M}_c \sim 4 \times 10^{-6}\,M_\odot\,yr^{-1}$, and is similar to the values suggested by the pulsation period and the $K$ amplitude.

The very high reddening value obtained for phase III supports our suggestion (Section 3.1 and 4.3) that the decline in the IR flux was caused by obscuration of the Mira by dust. A much shorter phase of increased reddening also occured in 1983/84. The possible causes of these events will be discussed later; however, the fact that the emission-line ratios and the UV continuum do not indicate any increase in the reddening implies that the site of the obscuration must be in the vicinity of the Mira component, leaving the hot component and the ionized region outside.

After ∼ JD 244 5000 the $K$ magnitude of RX Pup does not seem to be much affected by the hot component radiation, and can be used to estimate the distance via the period–luminosity relation (Feast et al. 1989; van Leeuwen et al. 1997):

$$M_K = 0.88 - 3.47 \log P. \quad (3)$$

Thus $M_K = -8.7$, although we note that this relation is not well-calibrated for long-period Miras. The average $K$ magnitude corrected for the respective values of $E(B-V)$ did not change in epoch II–IV; $< K_0 > = 2.64$, implying a distance of $d = 1.8 \pm 0.5$ kpc.

In summary, the above analysis is consistent with constant reddening, $E(B-V) \sim 0.8 \pm 0.2$ mag, towards the hot component and the ionized nebular region, with an additional variable reddening of $E(B-V) \sim 0$ to 2.5 mag towards the Mira. In the following analyses of the hot component and the ionized nebula, values of $E(B-V) = 0.8$ and $d = 1.8$ kpc are adopted.

## 3.3 Temperature and luminosity of the hot component

Three methods are used to determine the temperature, $T_h$, of the hot component. Wherever possible, $T_h$ is estimated from the observed equivalent width of the He II λ1640 emission line from *IUE* spectra, and the He II λ4686/H$\beta$ or He II λ4686/He I λ5876 ratios from

optical spectra. Since H$\beta$ may be weakened by optical depth effects, we assume that He II $\lambda$4686/He I $\lambda$5876 is a more reliable indicator of the temperature than He II $\lambda$4686/H$\beta$ for the period 1983–1990, when optical depth effects seem to be important. The third method applies the relation between $T_h$ and the highest observed ionization potential, $\chi_{max}$,

$$T_h[1000\,K] = \chi_{max}[eV], \quad (4)$$

proposed by Mürset & Nussbaumer (1994). The accuracy of this method is about 10 per cent provided that the highest ionization stage is indeed observable. The highest observed ionization stages as well as the derived temperatures at various epochs are presented in Table 6. The highest ionization stage observed in *IUE* spectra of RX Pup is that of $Mg^{+4}$, and in optical spectra those of $Fe^{+6}$ and $O^{+5}$; they suggest temperatures in good agreement with estimates based on other methods.

To derive the luminosity of hot component(s), $L_h$, the following methods are used.

(i) The optical and IR photometry obtained during visual maximum ($\sim$ JD 244 2500–4 000) suggests negligible contribution of the cool giant to the *UBV* magnitudes, while the *JHKL* magnitudes contain contributions from both the cool and the hot components. We assume that the IR magnitudes observed in epoch IV (see Section 3.2.4) represent those of the Mira component, and that the contribution of the hot component to the IR continuum was negligible at that time. To estimate the *JHKL* magnitudes of the hot component in remaining epochs, we simply subtracted the contribution of the Mira component from the observed values. The values for $L_h$ in the last column of Table 6 correspond to the integrated (UV)–optical–IR luminosity. We combined the *UBV* magnitudes for JD 244 2524 (Feast et al. 1977) with the *JHKL* data for JD 244 2520, and the *UBV* magnitudes for JD 244 3627 (Klutz 1979) with the *IUE* spectra taken on JD 244 3770 and the average IR data from epoch I.

**Table 6.** Hot component parameters for RX Pup.

| JD 24... | Ion | $T_h$ [K] | $L_h$ [$L_\odot$] | Method |
|---|---|---|---|---|
| 42524 | | 8 000 | 10700 | i |
| 43627-770 | | 9 000 | 18000 | i |
| 44055 | $He^{+2}$ | 80 000 | 8800 | ii |
| 44072 | $He^{+2}$ | 80 000 | 13800 | ii |
| 44345 | $Ne^{+4}$ | 100 000 | 15700 | ii |
| 44503 | $Ne^{+4}$ | 100 000 | 17600 | ii |
| 44767 | $Ne^{+4}$ | 110 000 | 17300 | ii |
| 45051 | $Ne^{+4}$ | 110 000 | 18300 | ii |
| 45459 | $Fe^{+6}$ | 120 000 | 17600 | ii |
| 45638 | $Mg^{+4}$ | 120 000 | 15400 | ii |
| 45771 | $Mg^{+4}$ | 120 000 | 15000 | ii |
| 46559 | $Mg^{+4}$ | 120 000 | 13100 | ii |
| 47459 | $Mg^{+4}$ | 120 000 | 10500 | ii |
| 47510 | | 120 000 | 7500 | ii |
| 47667 | $Mg^{+4}$ | 120 000 | 9100 | ii |
| 47893 | $O^{+5}$ | 115 000 | 3600 | iii |
| 47978 | | 115 000 | 3000 | iv |
| 48200 | $O^{+5}$ | 115 000 | 3600 | ii |
| 48215-23 | | 110 000 | 2700 | iv |
| 48328 | | 80 000 | 1000 | iv |
| 48328-85 | | | 550 | v |
| 48352 | $He^{+2}$ | 80 000 | 430 | ii |
| 48385 | $He^{+2}$ | 80 000 | 430 | ii |
| 49461 | $O^{+5}$ | 115 000 | $\lesssim$360 | iii |

(ii) Our second method is based on the flux of the He II $\lambda$1640 emission line measured from *IUE* spectra, or the He II $\lambda$4686, H$\beta$ and H$\alpha$ fluxes derived from optical spectra. We assumed a blackbody spectrum for the hot component, and that H I and He II emission lines are produced by photoionization followed by recombination (case B). The case B assumption is apparently not satisfied for the H I emission lines in 1983–1990, and thus the corresponding values for $L_h$ in Table 6 are those derived from He II, or, for JD 244 7510, from H$\alpha$, the flux of which should not differ from its case B value by more than 20 per cent (Netzer 1975). The He II $\lambda$1640 fluxes measured from low-resolution *IUE* spectra before 1983 have been corrected for the contribution of the O I] $\lambda$1641 line estimated from the high-resolution spectra. This contribution was $\sim$40 per cent of the total (He II $\lambda$1640 + O I] $\lambda$1641) flux in 1980 September, $\sim$30/25 per cent in 1981 June/1982 March, and becomes negligible after 1983 October.

(iii) Mikołajewska et al. (1997) found a relation between the hot component luminosity in symbiotic binary systems and the flux emitted in the Raman-scattered O VI $\lambda$6825 emission line. Schmid & Schild (1990b) report a weak emission at $\lambda \sim 6830$ Å on 1990 January 1, with an equivalent width of $\sim$11.7 Å which they identify as O VI $\lambda$6825. Similarly, Harries & Howarth (1996) estimate EW($\lambda$6825) $\sim 0.15 \pm .05$ Å in 1994 May. We converted these equivalent widths to fluxes estimating the continuum level from published $R_c$ photometry (Munari et al. 1992; IS94). O VI $\lambda$6825 was below our detection limit, $\sim 10^{-13}$ erg s$^{-1}$ cm$^{-2}$, in all our optical spectra, including those taken in November 1990.

(iv) In a few cases $L_h$ was derived from *UBV* magnitudes observed during the nebular phase. The method was proposed by Mürset & Nussbaumer (1994), who also gave the bolometric corrections to the *UBV* magnitudes for a wide range of $T_h$. For JD 244 7978 and JD 244 8215/23, published *UBV* magnitudes (Munari et al. 1992; IS94) were used, while for JD 244 8328, the *UBV* magnitudes were calculated from our *HST* spectrum.

(v) The *HST* spectrum was also used to calculate the integrated ($\lambda\lambda$1770 – 5450 Å) flux. The flux emitted shortwards of 1200 Å, $L_{EUV,h}$, can be estimated from the optical H$\beta$, He I $\lambda$5876 and He II $\lambda$4686 emission lines (Kenyon et al. 1991; their equation 8). The sum of the integrated *HST* flux and $L_{EUV,h}$ derived from the data in Table 3 for JD 244 8352 and 244 8385 agrees very well with the values indicated by the method (ii), and is lower by a factor of $\sim$2 than the value derived from *UBV* magnitudes (method iv).

We estimate that the luminosities in Table 6 have accuracies of a factor of 2, as indicated by the values obtained at the same epoch, but using different methods. In addition, there is a systematic error caused by uncertainties in reddening and distance estimates; this, however, should not affect any conclusions about the evolution of the hot component luminosity with time.

The data in Table 6 demonstrate that the hot component had roughly constant luminosity in 1975–1989, although its temperature changes by a factor of 15. Between 1989 May and 1991 April, $L_h$ dropped by a factor of $\sim$20, while $T_h$ decreased by $\gtrsim$40 per cent. The evolution of RX Pup in 1975–1991 thus parallels the evolution of a typical symbiotic nova (compare Mikołajewska & Kenyon 1992b; Kenyon et al. 1993; Mürset & Nussbaumer 1994).

In 1995–96, the optical continuum is much stronger than in 1991, while the nebular emission is significantly reduced. There is no evidence for high-ionization lines. In particular, we do not see He II $\lambda$4686 in a spectrum taken in 1996, and the upper limit for the equivalent width of the Raman-scattered O VI $\lambda$6825 emission line, EW($\lambda$6825) $\lesssim$0.15 Å, is comparable to the value measured in 1994

by Harries & Howarth (1996), and requires $L_h$ of the order of 100 $L_\odot$. On the other hand, RX Pup was detected by *ROSAT* in 1993 April/June (Mürset, Wolff & Jordan 1997), although the *IUE* spectrum from 1993 May does not show any evidence for high ionization features, nor does the optical spectrum from 1993 June (IS94) which is very similar to our 1995/96 spectra. The lack of measurable He II emission (for $T_h \gtrsim 10^5$ K and $L_h \sim 100\,L_\odot$ the observed flux in He II 4686 should be of $\sim 10^{-13}$ erg s$^{-1}$ cm$^{-2}$) may then be caused by obscuration of the He II formation region, which must be located very close to the hot component.

The H I Balmer emission lines are relatively strong, and their equivalent widths, EW(H$\alpha$) $\approx$ 200–250 Å and EW(H$\beta$) $\approx$ 16–24 Å, measured on our 1995–96 spectra, respectively, are comparable to those observed in the quiescent recurrent novae T CrB and RS Oph (Dobrzycka et al. 1996b; Anupama & Mikołajewska 1999). The He I emission lines are, however, very faint or absent. The colour temperature of the optical $\lambda\lambda$4500–5500 Å continuum is low, $T \sim 7000$–$6000$ K for $E(B-V) = 0.8$. This component has a luminosity of $L \sim 600(d/1.8\,\mathrm{kpc})^2\,L_\odot$. On the other hand, the optical emission lines indicate a higher temperature, $T \sim 2.5 - 4 \times 10^4$ K, with a roughly comparable luminosity, $L \sim 500$–$1000(d/1.8\,\mathrm{kpc})^2\,L_\odot$. We find here a striking similarity between RX Pup and the quiescent symbiotic recurrent novae RS Oph and T CrB, as well as the hot component of CH Cyg during bright phases. In all these systems, the optical data indicate the presence of a relatively cool F/A (CH Cyg) or A/B-type source (RS Oph and T CrB), while the optical emission lines indicate a higher temperature source, with a roughly comparable luminosity (Mikołajewska et al. 1988; Dobrzycka et al. 1996b; Anupama & Mikołajewska 1999). We will return to this problem in Section 4.

### 3.4 Nebular emission

The rich emission-line spectrum that has been developing since late 1979 offers various possibilities for the determination of the nebular parameters $T_e$ and $n_e$. Published estimates for the electron density indicate systematic differences between the values derived from the UV intercombination lines and those derived from the forbidden optical emission lines. In particular, K82 estimate $n_e \sim 10^{10}$ cm$^{-3}$ from *IUE* observations in 1981 June, while W84 derive $n_e \gtrsim 10^5$ and $\sim 10^7$ cm$^{-3}$ from the [S II] $\lambda$6717/$\lambda$6731 and [O III] $\lambda$4363/($\lambda$4959+$\lambda$5007) line intensity ratios, respectively, observed in 1983. Based on the optical spectrum taken in December 1989, FPC92 simulate the density gradient inside the ionized region by adopting a two-layer model, in which different ionization stages are present, and derive $n_e \sim 4.5 \times 10^6$ cm$^{-3}$ from high-excitation [O III] and [Fe VI] emission-line ratios, and $n_e \sim 2.6 \times 10^5$ cm$^{-3}$ from low-excitation [N II] and [S II] line ratios, respectively. All these estimates assume a photoionized region with $T_e \sim 10^4$ K.

The significance of the density gradient in the ionized region is also indicated by the O III]/[O III] line ratio. Nussbaumer & Storey (1979) demonstrated that simultaneous observations of the UV intercombination O III] $\lambda\lambda$1661, 1667 and optical forbidden [O III] $\lambda\lambda$4363, 4959, 5007 emission lines enable both $T_e$ and $n_e$ to be determined. Although the *IUE* and optical observations presented here are not simultaneous, we can combine the O III] $\lambda$1664 fluxes from Table 2 with published measurements for the optical [O III] lines. In particular, the 1983 [O III] fluxes from W84 combined with the mean of O III] $\lambda$1664 flux measured from the *IUE* spectra taken in 1982 and 1983 require a region with $n_e \sim 10^9$–$10^{10}$ cm$^{-3}$ and $T_e \sim 7500$ K for $E(B-V) \sim 0.8$–1. The O III]/[O III] intensity observed in the late 1980s (Table 2; van Winckel et al. 1993; FPC92) also require high densities and very low temperatures $T_e \lesssim 7000$ K. Such a low temperature is, however, in conflict with the absence of strong lines arising from dielectronic recombination. A similar effect is seen in other symbiotic systems, including symbiotic novae (e.g. Schmid & Schild 1990a). To solve this problem, Schmid & Schild inferred that the forbidden lines come from a much more extended region (by a factor of $10^4$ or so) than the O III] emission, both having similar $T_e \gtrsim 10^4$ K.

There is no simple method of determining $T_e$ in symbiotic systems. Nussbaumer & Storey (1984) have proposed the use of dielectronic recombination lines. The idea rests on a comparison of a collisionally excited line with one produced by dielectronic recombination. Nussbaumer & Storey also list promising recombination lines longwards of 912 Å. The best candidates among these are N IV $\lambda$1719 and C II $\lambda$1335. The observed flux ratio N V $\lambda$1240/N IV $\lambda$1719 grew from $\approx$1.5 in 1981 to $\approx$3 in 1984, and $\approx$8 in 1986. The corresponding temperatures are $T_e \approx 12\,000$ K in 1981, 13 000 K in 1984, and 15 000 K in 1986, for $E(B-V) \sim 0.8$. A very weak C II $\lambda$1335 line is present in spectra taken in 1979 and 1980. The observed flux ratios C III] $\lambda$1909/C II $\lambda$1335 $\sim$60 in 1979 and $\gtrsim$100 in 1980 indicate $T_e \sim 12\,000$–$13\,000$ K. These temperatures argue very strongly in favour of a radiatively ionized UV emission-line region.

The line ratios within the UV O IV] $\lambda$1401 and N III] $\lambda$1750 multiplets are very sensitive to $n_e$ (Nussbaumer & Storey 1979, 1982). The N III] $\lambda$1754/$\lambda$1749.7 and N III] $\lambda$1752.2/$\lambda$1749.7 ratios measured on *IUE* high-resolution spectra indicate that the electron density was decreasing from $n_e \gtrsim 10^{10}$–$10^{11}$ in 1980 to $\sim 5 \times 10^9$ in 1982–83 and $\sim 10^9$ cm$^{-3}$ in 1987. Similarly, we estimate $n_e \sim 10^{10}$ in 1981 and $\sim 10^9$ cm$^{-3}$ in 1987 from the O IV] $\lambda$1407.4/$\lambda$1404.8 ratio. These results are practically independent of $T_e$. We also observe a decreasing trend in the Si III] $\lambda$1892/C III] $\lambda$1908 and an increasing trend in the N III] $\lambda$1750/C III] $\lambda$1908 line ratios measured on the low-resolution *IUE* spectra. These trends can be interpreted as a continuously decreasing $n_e$. Finally, the increase in the C IV doublet ratio in 1980–1988 (see Section 3.1.2) is consistent with decreasing optical depth (which is related to density) in the high-excitation permitted line region.

We can now determine whether or not the parameters derived from the intercombination lines are also representative of the H I/He I emission region. The ionization potentials of $O^{+2}$ (54.9 eV) and $He^+$ (54.4 eV) are very similar, so He I and O III] should be emitted in the same physical region. The fluxes in He I $\lambda$5876 and O III] $\lambda$1664 then require $n_e \sim 10^{10}$ cm$^{-3}$ in 1983–84 and $n_e \sim 10^9$ cm$^{-3}$ in 1988/90, and $T_e \sim 15\,000$ K in 1984–90. The dependence of emissivity in He I $\lambda$5876 on $T_e$ and $n_e$ was taken from Proga et al. (1994) and Proga (private communication), while, for O III] $\lambda$1664, data from Nussbaumer & Storey (1981) were used. The volumes needed to account for the O III] $\lambda$1664 and He I 5876 emission fluxes are $V \sim 8 \times 10^{40}$ and $\sim 2 \times 10^{42}\,(d/1.8\,\mathrm{kpc})^2$ cm$^3$ in 1983–84 and 1988–90, respectively, so the corresponding radii are $R \sim 2$ and $\sim$5 au. The resulting emission measures are a factor of $\sim$2 higher than corresponding values derived from the H$\beta$, and roughly equal to those derived from the H$\alpha$ emission fluxes. However, these estimates assume that the H I lines follow case B. For a constant-density gas, the optical depth in H$\alpha$ is $\tau_{H\alpha} \approx 10(R/1\,\mathrm{au})/(n_e/10^{10}\,\mathrm{cm}^{-3})$ (Cox & Matthews 1969). We estimate $\tau_{H\alpha} \sim 20$ and $\sim$5 in 1983–84 and 1988–90, respectively. In such conditions the H$\beta$ flux could be reduced by $\sim$50–70 per cent with respect to the case B value, while H$\alpha$ should be somewhat (by $\lesssim 20$ per cent) enhanced. These results indicate that the UV intercombination lines form in the same gas as do the H I and He I lines.

Our spectra taken in 1991 do not show any measurable UV emission lines, while the optical H I, He I emission lines remain strong. The He I line ratios are consistent with formation in a region with $n_e \sim 10^6$–$10^8$ cm$^{-3}$ (Proga et al. 1994), while the H I line ratios are consistent with case B for $E(B-V) \sim 0.8$–1. We estimate the emission measure $n_e^2 V \sim 1.4 \times 10^{59}$ and $\sim 1.2 \times 10^{59}\,(d/1.8\,\mathrm{kpc})^2$ cm$^{-5}$, for the He I/H I line emitting region ($T_e \sim 15\,000$ K), and the expected O III] λ1664 flux is $\lesssim 7 \times 10^{-15}$ erg s$^{-1}$ cm$^{-2}$ which is below the detection limit for our *IUE* spectrum.

We now examine the low-density region in which the forbidden lines are produced. Based on an analysis of the forbidden lines in three symbiotic novae, Schmid & Schild (1990a) found that physical conditions vary strongly throughout the nebulosities. In particular, they found a steep electron density gradient from the lowest to the highest observed ionization stages. Following their suggestion, we have grouped the diagnostic line ratios used according to the ionizational potential of the ions involved:

(i) the transition region between the ionized and neutral gas, characterized by [S II] and [O I];
(ii) the $He^+$ zone and the outer edge of the $He^{+2}$ region, described by [N II], [Fe III], [Ar III], [O III] and [Ne IV]; and
(iii) the inner $He^{+2}$ region, characterized by [Ne V], [Mg V], [Fe VI] and [Fe VII].

The [S II] λ6716/λ6731 ratio is consistent with $n_e \sim$ few $\times 10^4$ cm$^{-3}$ and $T_e \sim 10^4$ K (Cantó et al. 1980) for the entire observing period. The electron temperature can be in principle constrained by [O I] (λ6300+λ6364)/λ5579 (Keenan et al. 1995), and the data in Table 3 are consistent with $n_e \sim 2 \times 10^4$ cm$^{-3}$ and $T_e \sim 10\,000$ K in 1991, and $n_e \sim 5 \times 10^4$ cm$^{-3}$ and a rather high $T_e \lesssim 18\,000$ K in 1995. However, [O I] λ5579 can be severely affected by the atmospheric airglow (Keenan et al. 1995) so the [O I] ratio only constrains an upper limit for $T_e$.

The strong [Ar III] λ7135 and very weak or absent [Ar III] λ5192 lines (Table 3; FPC92) also indicate low $T_e$. Our estimate of $I(\lambda7135)/I(\lambda5192) \gtrsim 100$ from the 1991 spectrum implies $T_e \lesssim 15\,000$ K for $E(B-V) \sim 0.8$ (Keenan, Johnson & Kingston 1988). Unfortunately, our 1990 spectrum does not cover the ∼λ 5200 Å region. The absence of [Ar III] λ5192 in table 2 of FPC92 suggests $T_e \lesssim 20\,000$ K in 1989. The [N II] λ6584/λ5755 ratio observed in 1989–91 indicates $n_e \gtrsim 1.5 \times 10^5$ cm$^{-3}$ for $T_e \lesssim 15\,000$ K (Kafatos & Lynch 1980). Similarly, we estimate $n_e \gtrsim 8 \times 10^6$, $\gtrsim 4 \times 10^6$ and $\gtrsim 2 \times 10^6$ cm$^{-3}$ from [O III] (λ5007+λ4959)/λ4363 observed in 1983 (W84), 1989 (FPC92) and 1991 (Table 3), respectively (Nussbaumer & Storey 1981), and $n_e \sim 5$–$9 \times 10^6$ cm$^{-3}$ from the [Ne IV] λ1602/λ2423 ratio measured in 1986–87 (Nussbaumer 1982). The [Fe III] intensities are consistent with $n_e \sim 10^5$–$10^6$ in 1990 and $n_e \sim 10^5$ cm$^{-3}$ in 1991, respectively (Keenan et al. 1993). The volume needed to account for $L$([O III] λ5007) is $V \sim 1.7 \times 10^{46}$, $1.6 \times 10^{46}$ and $6 \times 10^{45}\,(d/1.8\,\mathrm{kpc})^2$ cm$^3$ in 1983, 1988–90 and 1991, respectively, (Nussbaumer & Storey 1981), and the corresponding radii are $R \sim 107/103/75\,(d/1.8\,\mathrm{kpc})^{2/3}$ au for a spherically symmetric nebula.

There is also no evidence for high $T_e$ in the region where the emission lines with the highest ionization potential originate. [Mg V] λλ2784, 2930 are very strong in several *IUE* spectra taken in 1986–89; λ 2417 is, however, very weak or absent. Our estimate of $I(\lambda2784 + \lambda2930)/I(\lambda2417) \lesssim 30$ is consistent with $T_e \lesssim 20\,000$ K for $n_e \lesssim 10^8$ cm$^{-3}$, and $E(B-V) \sim 0.8$ (Kafatos & Lynch 1980). Similarly, the absence of [Ar V] λ4626 on our optical spectrum taken in 1990 implies the observed ratio [Ar V] $I$(λ6435+λ7005)/$I$(λ4626) $\lesssim 6$, and $T_e \lesssim 20\,000$ K for $n_e \lesssim 10^8$ cm$^{-3}$ and $E(B-V) \sim 0.8$. The [Fe VI] λ4967/λ4973 and [Fe VII] λ4967/λ4989 ratios measured on our 1990 spectrum are then consistent with $n_e \sim 10^6$–$10^7$ cm$^{-3}$ (Nussbaumer & Storey 1978; 1982). The volume needed to account for the luminosity in the [Fe VII] λλ6086, 5721 lines is then comparable to that required for [O III] lines if Fe/H is similar to that found in other symbiotic novae and M giants (e.g. Schmid & Schild 1990a).

The physical conditions in the nebula are thus consistent with those expected from a photoionized gas. The bulk of permitted and intercombination lines are formed in a dense region of ∼ a few au and $n_e \sim 10^9$–$10^{10}$ cm$^{-3}$, with an average $T_e \sim 15\,000$ K. The forbidden lines come from a more extended region of ∼100 au ([O III], [Fe VII]) or larger. We also find a steep density gradient covering more than two orders of magnitudes from the highest ($Fe^{+6}$) to the lowest ($S^+$) observed ionization stage in the forbidden-line emitting region. $T_e$ also decreases with decreasing ionization. The conditions in the nebula were evolving during the period under discussion. The average $T_e$ was increasing with increasing ionization level until c. 1989, then in 1991 it decreased in step with the ionization degree. The opposite trend is observed in $n_e$; it was slowly decreasing until c. 1989. In both the permitted/intercombination line emitting region and the forbidden line region, the average $n_e$ decreased by an order of magnitude. This trend is also manifested by a general increase in the forbidden emission-line fluxes with respect to the permitted lines with similar ionization potentials.

A comparison of the conditions derived from the H I, He I and O III] lines with those derived from the forbidden lines, [O III] and [Fe VII], suggests that the density gradient observed in RX Pup is roughly of a form $n_e \sim r^{-2}$, which is consistent with the emission from an ionized wind emanating from the system. A similar conclusion is reached from an analysis of the radio observations (Hollis et al. 1986; Seaquist & Taylor 1987, 1992). This shows the spectrum and angular structure expected from partially optically thick thermal bremsstrahlung originating in a spherically symmetric steady stellar wind. The cm–mm spectrum observed in 1985–1988 is essentially linear from 1.49 to 394 GHz, and is well represented by a spectrum of the form $S_\nu = 9.9\,\nu^{0.80}$ mJy (Seaquist & Taylor 1992). The photospheric radius at 394 GHz is given by $r \sim 29\,(d/1.8\mathrm{kpc})$ au, and the turnover frequency $\nu_t \gtrsim 394$ GHz implies $n_e \gtrsim 8 \times 10^7$ cm$^{-3}$ inside that radius.

For a spherically symmetric steady wind emanating predominantly either from the cool giant or the hot companion, we have

$$n_e = \frac{\dot{M}}{4\pi\mu m_H v r^2}, \qquad (5)$$

where $r$ is the radial distance from the centre of the star, $\mu$ the mean atomic weight of the gas and $m_H$ the mass of a hydrogen atom. Using the characteristic radii and densities derived above from the emission lines and radio–mm data for 1985–88, we estimate $\dot{M}/v \sim 6 \times 10^{-6}$ [$M_\odot$ yr$^{-1}$/100 km s$^{-1}$]. FW's analysis of emission line profiles indicates $v \sim 140$ km s$^{-1}$ and $\dot{M} \sim 10^{-5}\,M_\odot$ yr$^{-1}$. It is unlikely that the cool giant wind has a velocity in excess of 100 km s$^{-1}$. We thus assume the wind originates from the hot star. The evolution in the nebular conditions can then reflect the changes in that wind. Note that our estimate for $\dot{M}$, although acceptable for a symbiotic nova (e.g. Kato 1997), is very approximate. In particular, there is evidence for elongated structure in the radio and optical emission lines (Hollis et al. 1986; Paresce 1990), which indicates that the wind may be bipolar. The observed radio spectral index of

$\sim +0.8$ also departs from the canonical value of +0.6 expected for a spherically symmetric wind.

The change in the emission spectrum in 1991 can be understood in terms of decreased $\dot{M}$ and gradual recombination in the ionized region following the decline in the hot component luminosity, which is no longer able to maintain the ionization of the wind. As the recombination time-scale, $\tau_{\rm rec}$, is inversely proportional to $n_{\rm e}$ – $\tau_{\rm rec} \sim 1$ h/1 month/15 yr for $n_{\rm e} \sim 10^9/10^6/10^4$ cm$^{-3}$, respectively, the inner portions of the winds are the first to recombine. In fact, spectra taken in 1995 and 1996 show low-ionization emission lines of [O I], [S II], [N II] with almost the same (within a factor of $\sim$2) intensity as observed in 1990 and 1991, and very faint [O III] lines; all these lines have intensities roughly consistent with their originating in a region with $n_{\rm e} \sim 10^4$ cm$^{-3}$ and $T_{\rm e} \lesssim 10\,000$ K. Such a scenario is also consistent with the observed changes in radio emission. This suggested an optically thick wind emanating from the system in the 1980s, while since c. 1991 it is better understood as optically thin emission (IS94, and references therein) arising from the low-density remnant of the 1980–90 high-ionization phase.

Only the Balmer H I and Fe II emission lines show increased intensity in our 1995/96 spectra. This increase coincides with the appearance of an A/F-type continuum source. The very steep Balmer decrement is consistent with its origin in a relatively dense region, $n_{\rm e} \gtrsim 10^{10}$ cm$^{-3}$ (Drake & Ulrich 1980). Assuming $T_{\rm e} \lesssim 10^4$ K, we estimate the optically thin emission measure $n_{\rm e}^2 V \sim 4 \times 10^{59} (d/1.8\,{\rm kpc})^2$ cm$^{-3}$ from the H$\beta$ and H$\alpha$ emission-line fluxes. Again, we emphasize here the similarity to the spectroscopic appearance of CH Cyg during its active phases. In particular, the luminosity of the A/F-type continuum, as well as the conditions (density, emission measure) in the H II Balmer emission region at maximum of CH Cyg's activity (Mikołajewska et al. 1987, 1988) are comparable to those derived from the 1995/96 spectra of RX Pup.

## 4 DISCUSSION

### 4.1 Geometrical configuration of RX Pup

The large difference between the reddening towards the Mira component and the reddening towards the hot component and ionized region indicates that the hot component and most of the ionized material must lie along a line of sight that does not include the Mira variable and its associated dust cocoon.

Kenyon, Fernandez-Castro & Stencel (1988) deduced a characteristic dust radius of $\sim$200 au from *IRAS* colours, while Anandarao, Taylor & Pottasch (1988) derived a dust shell radius of $\sim$77 au (rescaled for our adopted distance of 1.8 kpc) from analysis of the *IRAS* photometry and low-resolution spectroscopy. Both values are an order of magnitude larger than the binary separation, $a \sim 17$ au, suggested by the IS94 model.

Schmid & Schild (1990b) report weak emission at $\lambda$ 6825 Å in 1990 January resulting from Raman-scattering of the O VI $\lambda$ 1032 resonance line. They also noted that the lack of detectable polarization in this line indicates that the line of sight coincides roughly with the direction defined by the $O^{+5}$ zone and the Mira variable. RX Pup shows at the same epoch very strong [Fe VII] emission lines, and the lack of strongly scattered O VI $\lambda$ 6825 emission is unusual. Practically *all* symbiotic systems with strong [Fe VII] lines also have strong O VI $\lambda\lambda$ 6825, 7082 lines (Kenyon 1986; Mikołajewska et al. 1997). The apparent weakness of the Raman-scattered O VI line suggests that the scattering process in the envelope of RX Pup must be very inefficient, probably due to insufficient numbers of the scatterers – neutral hydrogen atoms. Theoretical simulations of the Raman scattering in symbiotic systems demonstrated that the process has the highest efficiency in systems having ionization geometry with an $X$-parameter (as defined by Seaquist, Taylor & Button 1984, hereafter STB84) of $X \sim 1$, while in systems with $X \gtrsim 5$, the efficiency is much lower (Schmid 1996). The weak O VI $\lambda$ 6825 would thus suggest that in RX Pup only a cone-shaped region shielded by dense material surrounding the Mira component remains neutral, while the lack of measurable polarization indicates that in 1990 the $O^{+5}$ zone (and the hot component) was in front of this neutral region. Moreover, the lack of changes in the reddening towards the hot component and the nebular region (Section 3.2) shows that, at least during the last 18 yr, both the hot component and the emission-line region have remained outside the dust shell of the Mira component. In particular, this rules out the possibility that the changes in the extinction towards the Mira component are orbitally related (we return to this problem in Section 4.3).

The conical shape of the interface between neutral and ionized regions in RX Pup can be produced either by illumination of the wind of the Mira component by the hot companion (STB84) or by interacting winds (Girard & Willson 1987). We have already demonstrated that the nebular emission in RX Pup originates from an ionized wind emanating from the system, and that the hot component is the most likely source of this wind. One can expect that this wind will interact with the wind of the Mira component. Assuming that the shock front coincides with the interface between the ionized and neutral regions, then $X \gtrsim 5$ (see above) corresponds to a momentum ratio $mv = \dot{M}_{\rm h} v_{\rm h} / \dot{M}_{\rm c} v_{\rm c} \gtrsim 10$. Adopting $\dot{M}_{\rm h} \sim 10^{-5}\,{\rm M}_\odot\,{\rm yr}^{-1}$, $v_{\rm h} \sim 140\,{\rm km\,s}^{-1}$ (Section 3.4), $\dot{M}_{\rm c} \sim 4 \times 10^{-6}\,{\rm M}_\odot\,{\rm yr}^{-1}$ (Section 3.2.4), and assuming reasonable $v_{\rm c} \sim 20\,{\rm km\,s}^{-1}$ (Whitelock et al. 1994), we estimate $mv \sim 18$, in agreement with the suggested geometry. The distance of the shock from the Mira normalized to the binary separation will then be $\sim$0.2. The latter result combined with the fact that the Mira component is never stripped of its dust envelope (Table 5) implies a binary separation that is a factor of $\sim$5 or so larger than the dust formation radius. Assuming a typical dust formation radius of $\gtrsim 5 \times R_{\rm c}$, and a Mira radius $R_{\rm c} \sim 2$–3 au (e.g. Haniff, Scholz & Tuthill 1995), the required binary separation is $a \gtrsim 50$ au.

With so large a binary separation, the Mira in RX Pup should have SiO masers, whereas the search for such emission in 1987 (43 GHz; Allen et al. 1989), 1989 and 1994 (86 GHz; Schwarz et al. 1995) resulted in an upper limit that was a factor of $\sim$100 below fluxes in single Mira variables with similar pulsation periods. The popular explanations for the apparent absence of SiO masers (as well as OH and $H_2O$) in most symbiotic systems involve radiation or tidal effects related to the hot compact companion (Schwarz et al. 1995, and references therein). These are unlikely to apply to RX Pup, mostly because of the large binary separation, but also because a significant amount of the circumstellar dust is always present outside the SiO formation region (if the SiO molecules are destroyed by hot radiation the dust should be destroyed too). Moreover, at least the 1994 observation was made after the luminosity and temperature of the companion significantly decreased.

Allen et al. (1989) noted that if the cool giant were always viewed through the ionized nebula, then the masers would be obscured at frequencies for which the nebula is optically thick. Moreover, Nyman & Olofsson (1986) found a correlation of the 87-GHz flux with the Mira pulsation phase. In fact, these two effects can explain the failure to detect SiO masers in RX Pup. First, our analysis suggests the Mira component was always viewed through the

ionized nebula. Thus in 1987, when the optically thick radio emission up to ≳300 GHz was observed (IS94), the 43-GHz maser would indeed be obscured. It seems that the radio spectrum remained optically thick until c. 1991 (IS94), which indicates that in 1989 the 87-GHz maser could also have been obscured. Although the nebula was optically thin at 87 GHz, at least in 1994, both the 1989 and 1994 observations were made near the Mira minimum ($\phi \approx 0.42$ and $\phi \approx 0.48$, respectively). The lack of detectable SiO masers in RX Pup is therefore consistent with the suggested geometrical configuration of this system. It also seems reasonable to repeat the search for such emission near to the Mira maximum, and when the system is in a low-excitation stage with a flat radio spectrum.

### 4.2 Evolution of the hot component

Fig. 11 shows the evolution of the hot component in the Hertzsprung–Russell (HR) diagram – for the luminosities and temperatures derived in Section 3.3 – along with the cooling curves for 0.64- and 0.55-$M_\odot$ white dwarfs, respectively. The hot component appears to maintain a constant bolometric luminosity, $< L_h >= 15\,000 \pm 1\,000\,L_\odot$, from 1975 to 1986, though its temperature varies by a factor ≳15. In 1988/89 it turned over in the HR diagram; since then our estimates suggest a decline in luminosity initially at roughly constant temperature. Between 1989 May and 1991 April, $L_h$ dropped by a factor of ∼20, while $T_h$ decreased by ≳40 per cent. The evolution of RX Pup during its recent active phase thus parallels the evolution of a typical symbiotic nova, pointing to a thermonuclear nova eruption (compare Mikołajewska & Kenyon 1992b; Kenyon et al. 1993; Mürset & Nussbaumer 1994), and in particular it rules out the accretion model proposed by K85, with its recent development by IS94. Neither can the accretion model account for the emission-line profiles or the evolution of the radio spectrum (see Section 3.4 for details). The evolution of $L_h$ is also inconsistent with the thermonuclear runaway model proposed by AW88, which assumes a very slow hydrogen-shell flash with a plateau phase lasting decades. In particular, the AW88 model does not predict any significant changes in $L_h$, as all photometric and spectral changes have been attributed to changes in the mass loss from the white dwarf.

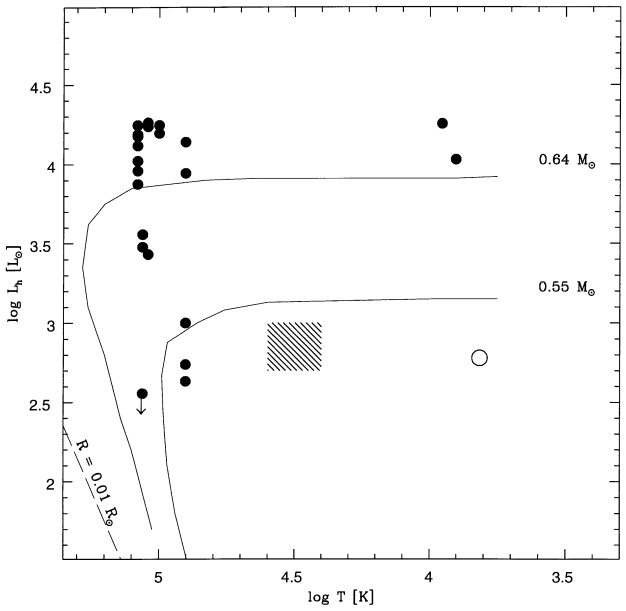


**Figure 11.** Evolution of the hot component in the HR diagram in 1975–1996. Dots indicate the 1975–1994 outburst cycle. The shaded square represents the results derived from H I emission lines, while the open circle locates the A/F-type component observed in 1995–96. The solid curves are the evolutionary tracks from Schönberner (1989), the dashed curve is a line of constant radius.

The estimated maximum bolometric luminosity, $L_h \approx 15\,000\,L_\odot$, falls within the range of plateau luminosities for other symbiotic novae (Mikołajewska & Kenyon 1992b; Mürset & Nussbaumer 1994). Applying the relationship between plateau luminosity and white dwarf mass for accreting cold white dwarfs from Iben & Tutukov (1996, their equation 8), we estimate the mass of the white dwarf in RX Pup, $m_{WD} \sim 0.59\,M_\odot$, while the Paczyński–Uus relation (Paczyński 1970; Uus 1970) gives $m_{WD} \sim 0.77\,M_\odot$. The luminosity–mass relation during the plateau phase, however, depends significantly on the thermal history of the white dwarf: generally hot white dwarfs must have larger masses than the cool ones to reach the same luminosity during a hydrogen-burning phase (Iben & Tutukov 1996). Our estimates for the white dwarf mass of RX Pup should thus be considered as lower limits.

RX Pup may be the first recurrent nova detected in a D-type symbiotic system. Published observations suggest that RX Pup was visually bright in 1894, and its spectrum resembled that of $\eta$ Car, with strong H I Balmer emission lines (Pickering 1897). Three years later a high-excitation nebular spectrum emerged, with strong emission lines of He II, [O III] and [Ne III], in addition to the H I Balmer series (Cannon 1916). After 1900, RX Pup entered a deep optical minimum ($m_{pg} = 14.1$ mag in 1904–5; Pickering 1914) resembling that in 1991. The star recovered from the minimum in 1909, and from then up until 1924 it showed only small fluctuations around $m_{pg} \sim 12$ mag (Yamamoto 1924). The high-excitation spectrum was again observed in 1941 (Swings & Struve 1941), while in 1949–51 the excitation level was moderate and the optical continuum was very weak (Henize 1976). In the late 1960s RX Pup remained very faint optically ($m_{vis} = 12.5, m_{pg} = 13.5$) and the high-excitation features were absent (Sanduleak & Stephenson 1973). In 1969/70 the $V$ magnitude brightened to 9.4 mag (Eggen 1973), and the recent outburst began. The historical records of RX Pup thus suggest that around 1894 it underwent another nova-like eruption. Unfortunately, the lack of observations in the 1930s makes it impossible for us to ascertain whether the presence of a high-excitation spectrum in 1941 was also due to the eruption.

The recurrence time for RX Pup, $\tau_{rec} \sim 80(40)$ yr, is comparable to that of two symbiotic recurrent novae, T CrB (80 yr) and RS Oph (22 yr), and it requires an accretion rate of the order of $\sim 10^{-7}\,M_\odot\,yr^{-1}$ (Prialnik & Kovetz 1995). According to Bondi–Hoyle theory, even in a wide binary system a white dwarf can accrete as much as ∼1 per cent of the stellar wind of the giant (Livio 1988, and references therein), which in the case of RX Pup is just what is needed. The observed quiescent luminosities of the compact components of the Mira AB (∼2 $L_\odot$; Karovska et al. 1997)[2] and R Aqr (a few $L_\odot$; Michalitsianos, Kafatos & Hobbs 1980) spatially resolved wind-accreting binary systems agree with the values predicted by the accretion theory. The component separation of Mira AB, $a\sim$ 70 au (Karovska et al. 1997), is comparable to that expected for RX Pup, while the quiescent $L_h$ in RX Pup is a factor of ∼100 higher than that of Mira B, in good agreement with more or less the same order-of-magnitude difference in the mass-loss rates

[2]Their original values are scaled to the photometric parallax, 118 pc (e.g. van Leeuwen et al. 1997), which is in good agreement with the *Hipparcos* trigonometric parallax.

of the Mira in RX Pup ($\dot{M}_c \sim 4 \times 10^{-6}\,M_\odot\,yr^{-1}$; Section 3.2.4) and that of Mira A ($\dot{M}_c \sim 10^{-7}\,M_\odot\,yr^{-1}$; Reimers & Cassatella 1985).

The observed maximum luminosity as well as the very slow evolution in the HR diagram indicate a white dwarf mass significantly less than the $M_h \sim 1.4\,M_\odot$ usually expected for recurrent novae (e.g. Webbink et al. 1987). As the estimated $L_h$ is based largely on UV emission-line fluxes, it will be underestimated if the nebula is not ionization-bounded. However, any underestimate is unlikely to be sufficient to increase the white dwarf mass above $\sim 1\,M_\odot$. Moreover, recent model calculations show that while recurrent novae require high mass-accretion rates, $\dot{M} \gtrsim 10^{-8}\,M_\odot\,yr^{-1}$, the constraint on the white dwarf mass is less severe (Prialnik & Kovetz 1995). Short recurrence times can be obtained for white dwarf masses as low as $\sim 1 M_\odot$. Consequently, the decline times of recurrent nova models are not necessarily short. Given all the uncertainties involved in the theoretical modelling of symbiotic and recurrent novae (Sion 1997, and references therein), it seems plausible to suggest that RX Pup is a recurrent nova.

The quiescent hot component of RX Pup shows striking similarities to its counterparts in RS Oph and T CrB. In particular, the *ROSAT* spectrum of RX Pup observed in 1993 April–June (Mürset et al. 1997) is very similar to the *ROSAT* spectrum of RS Oph (Orio 1993); both show $\beta$-type spectra (according to the classification of Mürset et al.) compatible with emission from an optically thin plasma with a temperature of a few $10^6$ K. Mürset et al. suggest that such emission is due to hot shocked gas, and propose that the shock arises in the region where the strong and fast wind from the hot component crashes into the cool giant or its wind. Such an interpretation is, however, entirely incompatible with the observed properties of both RX Pup and RS Oph at the time of the *ROSAT* observations. The colliding wind model requires $L_h \sim 10\,000\,L_\odot$ for RX Pup, and $\sim 2000\,L_\odot$ for RS Oph, which is much higher that the observed $L_h \lesssim 1000\,L_\odot$ in RX Pup and $\sim 100$–$600\,L_\odot$ in RS Oph (Dobrzycka et al. 1996b). Moreover, the optical spectrum of RS Oph at that time was very similar to the quiescent (1993–96) spectrum of RX Pup, showing only weak low-ionization and low-excitation emission lines (Dobrzycka et al. 1996b).

It thus seems reasonable to assume (as did Orio for RS Oph) that the X-ray emission arises in the accretion flow. Assuming that the *ROSAT* flux represents a significant fraction of the total flux in the 0.2–4 keV range, a mass accretion rate $\dot{M}_{acc} \approx 10^{-9}(M_{WD}/0.7\,M_\odot)^{-1.8} M_\odot\,yr^{-1}$ (Patterson & Raymond 1985) can be estimated. However, this should be considered a lower limit to $\dot{M}_{acc}$, because the X-ray luminosity for RX Pup given by Mürset et al. was derived assuming a much lower reddening, $E(B-V) = 0.55$, than that derived above. In addition, local material might absorb a substantial fraction of the X-rays produced close to the white dwarf surface.

The quiescent optical spectrum of RX Pup, in particular the presence of a variable relatively cool F-type continuum with strong H I Balmer emission lines, also resembles the optical spectra of RS Oph and T CrB. These stars show an additional variable component in the optical–UV and sometimes also at IR wavelengths. For example, in RS Oph the IR colours indicate the presence of an additional warm, $\gtrsim$7000 K source (Evans et al. 1988), while Dobrzycka et al. (1996b) found an A–B type shell source with $L \sim 100$–$600\,L_\odot$, accompanied by strong H I and moderate He I emission lines. Similarly, Selvelli, Cassatella & Gilmozzi (1992; also Belczyński & Mikołajewska 1998; Anupama & Mikołajewska 1999) reported variable UV/optical continuum with $L \sim 40$–$100\,L_\odot$ in T CrB. Although both in the symbiotic recurrent novae T CrB and RS Oph and in RX Pup the average luminosity of the B/A/F-type shell source is consistent with the accretion rate, $\dot{M} \gtrsim 10^{-8}\,M_\odot\,yr^{-1}$, required by the theoretical models, the effective temperatures places the hot components far from the standard massive white dwarf tracks in the HR diagram. Simultaneously, the X-ray data suggest accretion rates that are 1–2 orders of magnitude lower. All three systems show similar quiescent behaviour: their hot components have highly variable luminosity and occasionally display blueshifted absorption features (see also Dobrzycka et al. 1996b; Anupama & Mikołajewska 1999).

It is also interesting that the shell spectrum appears only during the late decline from the nova outburst. In particular, the optical/visual light curves from the outbursts of T CrB, RS Oph and RX Pup show more or less pronounced minima followed by a standstill (or secondary maximum) associated with the appearance of the shell spectrum. We suggest that the minima are caused by a decline in the luminosity of the hot component after it passes the turnover in the HR diagram. The strong hot component wind during the plateau phase prevents accretion on to the hot component. Following the decline in luminosity the wind also ceases, and accretion of the material from the cool giant can be restored. We believe that the shell-type features and variable 'false atmosphere' observed at quiescence together with the H I emission-line spectrum originate from the accretion flow. The observed variability could be caused by fluctuations in the mass-loss rate from the cool giant; the shell spectrum becomes stronger as $\dot{M}_c$ increases and as a result $\dot{M}_{acc}$ increases. Finally, we recall the behaviour of CH Cyg, a highly variable symbiotic system containing an accreting white dwarf. The hot component luminosity in this system varies by a factor of $10^4$ (Mikołajewska 1994), between $\sim$0.1 and $\sim 300\,L_\odot$. The brightening of the hot component is associated with the presence of a flickering, which suggests that the system is accretion-powered. The optical/UV spectrum of CH Cyg during bright phases resembles the quiescent spectra of symbiotic recurrent novae (see also Section 3.3), while the detection of hard X-ray emission (Mürset et al. 1997; Ezuka, Ishida & Makino 1998) indicates that the accreting component is a white dwarf.

### 4.3 Obscuration of the Mira component

The light curves of symbiotic Miras were discussed by Whitelock (1987, 1988). RX Pup is typical of these in that it shows significant long-term variations (referred to as 'obscuration events' by Whitelock) in addition to the Mira pulsation. Fig. 12 shows the $J$ and $L$ light curves after removal of the Mira pulsations. This is done by subtracting the best-fitting 578-d sine curve from the data as displayed in Table 4 and Fig. 4. Only $J$ and $L$ are illustrated as they represent the extremes of behaviour. During the first approximately 2000 d, low-amplitude 578-d variations can be seen in antiphase with the pulsation cycle; these are artefacts of the pulsation removal process introduced by the lower amplitude of the Mira at that stage (see Section 3.2.4). The $\Delta J$ curve changes over a full range of about 2.5 mag, while the $\Delta L$ light curve shows a much lower amplitude, $\sim$0.8 mag, trend, with a minimum at the same time as the $\Delta J$ curve.

Although the light curves in Fig. 12 seem qualitatively similar to the visual light curve (Fig. 4), the optical minimum around JD 244 8300 can be accounted for by the evolution of the hot component, in particular the general decline in the emission-line spectrum (the change in emission-line fluxes alone can account for a $\sim$1/1.5 mag drop in $V/B$ magnitudes, respectively; Section 3.1) following the decrease in its luminosity. In fact, the visual magnitudes are generally not correlated with the IR magnitude, although

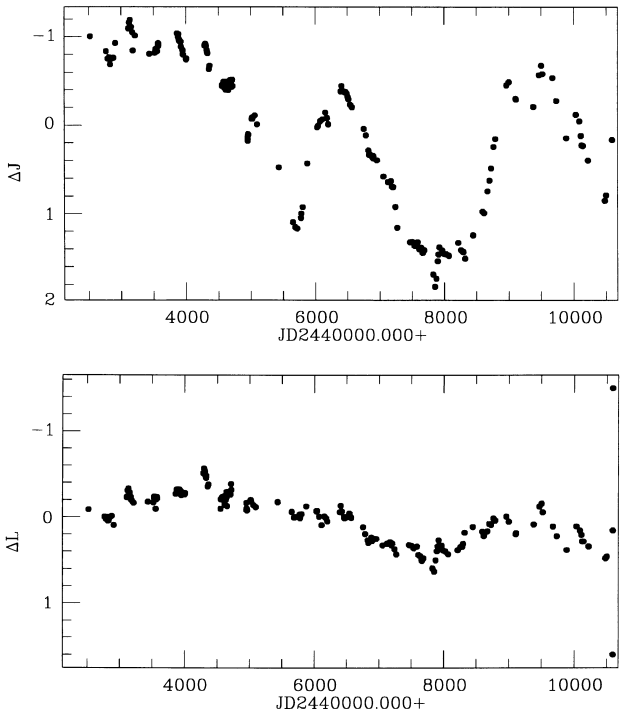


**Figure 12.** *J* and *L* light curves after the removal of the Mira pulsation.

the hot component may contribute to the IR before ~ JD 244 4000 (epoch I/optical maximum; see Section 3.2.4). In particular, the visual light curve was practically flat during JD 244 5000–8200, while the IR light curves showed pronounced changes (Fig. 12). Similarly, the decrease in IR flux after ~ JD 244 9500 is not accompanied by any related changes in the visual. This and the fact that the changes in the reddening towards the Mira are *not* correlated with similar changes in the reddening towards the hot component and emission-line formation region(s) strongly suggest the obscuration affects only the Mira component.

The physical nature of this phenomenon remains a mystery. In the specific case of the symbiotic star R Aqr the long-term trends were explained as the effect of an orbitally related eclipse of the Mira by pre-existing dust (Whitelock et al. 1983b). However, more recently Whitelock et al. (1997) have explained large-amplitude erratic variations in the light curves of carbon-rich Miras as the consequence of the ejection of puffs of dust by the star. The wavelength dependence of these two effects, an eclipse by pre-existing dust and the ejection of new dust, are very similar and it is difficult to determine which is occurring in RX Pup. From Fig. 12 it is clear that any eclipsing dust cloud would have to be very patchy, much more so than the cloud responsible for the eclipse in R Aqr.

Fig. 12 suggests a modulation with a time-scale of ~3000 d, while the reddening towards the hot component was practically constant over at least 13 yr. It is hard to imagine a geometry of the binary system in which the cool component is eclipsed at least twice while the hot component is not eclipsed at all. Thus, for RX Pup, it seem unlikely that the obscuration is orbitally related. Now that data are available over a longer time base it seems that the obscuration events occur in many symbiotic Miras with too great a frequency to be generally associated with binary eclipses (Whitelock 1999).

Although the most pronounced obscuration event coincides with the hot component passing the turnover in the HR diagram, the obscuration is apparently not associated with this component. In particular, the dust does not form in the material ejected from the hot component. The relative intensities of Si IV λ 1394 + O IV] λ 1403/N IV λ 1487 and O III] λ 1664/N III λ 1750 should not vary with changes in $T_h$, $n_e$ and ionization. The *IUE* data in Table 2 show that in RX Pup these ratios are roughly constant until at least JD 244 7667 which means that at that time O and Si are not being depleted by condensation into dust grains (silicates). Similarly, there is no indication for carbon depletion in the ejecta. Moreover, the absence of strong O I during the late outburst phase and the steady decline in He II emission suggest that the hot component ejecta lack a neutral zone. Similarly, Schmid & Schild (1990a) do not find evidence for significant depletion of Si and Fe in the ionized ejecta of V1016 Cyg and HM Sge, while Munari & Whitelock (1989) did not find any major changes of emission-line strengths associated with the dust obscuration episode in HM Sge.

The site of the dust responsible for the symbiotic Mira obscuration must be located in its circumstellar envelope. In a considerable number of Mira variables, the visual light curves exhibit complex variations from cycle to cycle as well as on long time-scales. Although the long-term modulations are more evident in C-rich Miras (e.g. R For, RU Vir), they are also present in the light curves of longer (≳300 d) period O-rich Miras (S CMi, R Hya; Mattei 1997). Longer period Miras generally have more dust and it seems likely that the long-term modulation of their light curves is related to the behaviour of this dust. Because they have more dust they are visually fainter and therefore less well studied at short wavelengths. It is therefore possible that these obscuration events have been easily recognized in symbiotic Miras simply because their light curves have been more extensively studied. Whitelock's (1999) discussion suggests that this is not the case, but more extensive studies are necessary to confirm this.

It is not at all clear how, or if, the obscuration events affect the rest of the symbiotic system. It is possible that an enhancement in the Mira wind produces a coordinated increase in the accretion luminosity of the hot component as suggested by the rise in the optical continuum and H I emission lines after ~ JD 245 0000 (Section 3.3). A similar relation between the obscuration of the Mira (and related enhancement in its wind) and an increase in the hot component luminosity is probably observed in R Aqr (Mikołajewska & Kenyon 1992b).

## 5 CONCLUSIONS

RX Pup is a long-period interacting binary system consisting of a Mira variable pulsating with $P \approx 578$ d, and a white dwarf companion. The binary separation could be as large as $a \gtrsim 50$ au (corresponding to $P_{orb} \gtrsim 200$ yr) as suggested by the permanent presence of a dust shell around the Mira component. In particular, the Mira component is never stripped of its dust envelope, contrary to the model proposed by IS94, and even during bright (not obscured) IR phases the star resembles high-mass-loss Galactic Miras with thick dust shells.

The analysis of multifrequency observations shows that most, if not all, photometric and spectroscopic activity of RX Pup in the UV, optical and radio range is caused by activity of the hot component, while the Mira variable and its circumstellar environment are responsible for practically all changes in the IR range. In particular, the evolution of the hot component in the HR diagram as well as evolution of the nebular emission in 1970–1993 is consistent with a symbiotic nova eruption, with the luminosity plateau reached in 1972/75 and a turnover in 1988/89. The hot component contracted in radius at roughly constant luminosity from c. 1972 to 1986;

during this phase it was the source of a strong stellar wind and therefore could not accrete any further material. By 1991 the luminosity of the nova remnant had decreased to a few per cent of the maximum (plateau) luminosity, and the hot wind had practically ceased. By 1995 the hot component started to accrete material from the Mira wind, as indicated by a general increase of the optical continuum and Balmer H I emission. The quiescent optical spectrum of RX Pup resembles the quiescent spectra of symbiotic recurrent novae, while the hot component luminosity is consistent with variable wind-accretion at a high rate, $\dot{M}_{\rm acc} \sim 10^{-7}\,{\rm M}_{\odot}\,{\rm yr}^{-1}$ ($\approx$1 per cent of $\dot{M}_{\rm c}$). RX Pup may be a recurrent nova; there is some evidence that a previous eruption occurred around 1894. The proposed binary model for RX Pup could be verified if flickering of the accretion disc were detected at quiescence. Such flickering has been observed in the symbiotic recurrent novae RS Oph and T CrB during quiescence, and in the accretion-powered symbiotic systems CH Cyg and MWC 560 (e.g. Dobrzycka, Kenyon & Milone 1996a).

Large changes were found in the reddening towards the Mira component; these were accompanied by fading of the near-IR flux. However, the reddening towards the hot component and emission-line regions remained practically constant and was generally less than that towards the Mira. These changes do not seem related to the orbital configuration or the hot component activity. The IR dust obscuration episodes are best explained as intrinsic changes in the circumstellar environment of the Mira component, possibly because of a variable mass-loss rate.

## ACKNOWLEDGMENTS

We gratefully acknowledge the very helpful comments on this project by W. Dziembowski, A. Nota, F. Paresce and R. Szczerba. We thank the variable star section of the Royal Astronomical Society of New Zealand for providing us with their visual magnitudes. We also thank the following people for making IR observations: Michael Feast, Brian Carter, Greg Roberts, Robin Catchpole and Dave Laney. This research was partly supported by KBN Research Grant No. 2 P03D 021 12.

## REFERENCES

Allen D. A., Wright A. E., 1988, MNRAS, 232, 683 (AW88)
Allen D. A., Hall P. J., Norris R. P., Troup E. R., Wark R. M., Wright A. E., 1989, MNRAS, 236, 363
Anandarao B. G., Taylor A. R., Pottasch S. R., 1988, A&A, 203, 361
Andrillat Y., 1982, in Friedjung M., Viotti, R., eds, The Nature of Symbiotic Stars. Reidel, Dordrecht, p. 47
Anupama G. C., Mikołajewska J., 1999, A&A, in press, astro-ph/9812432
Baldwin J. A., Stone R. P. S., 1984, MNRAS, 206, 241
Barton J. R., Phillips B. A., Allen D. A., 1979, MNRAS, 187, 813
Belczyński K., Mikołajewska J., 1998, MNRAS, 296, 77
Bromage G. E., Nandy K., 1973, A&A, 26, 17
Cannon A. J., 1916, Ann. Harv. Coll. Obs., 76, 19
Cantó J., Elliott K. H., Meaburn J., Theokas A. C., 1980, MNRAS, 193, 911
Carter B. S., 1990, MNRAS, 242, 1
Cassatella A., Ponz D., Selvelli P. L., 1982, NASA IUE Newsl., 10, 31
Chaffee F. H., Jr, White R. E., 1982, ApJS, 50, 169
Clavel J., Gilmozzi R., Prieto A., 1986, NASA IUE Newsl., 31, 83
Cox D. P, Mathews W. G., 1969, ApJ, 155, 859
de Freitas Pacheco J. A., Costa R. D. D., 1992, A&A, 257, 619 (FPC92)
Dobrzycka D., Kenyon S. J., Milone A. A. E., 1996a, AJ, 111, 414
Dobrzycka D., Kenyon S. J., Proga D., Mikołajewska J., Wade R. A., 1996b, AJ, 111, 2090
Drake S. A., Ulrich R. K., 1980, ApJS, 42, 351
Eggen O. J., 1973, PASP, 85, 42
Evans A., Callus C. M., Albinson J. S., Whitelock P. A., Glass I. S., Carter B., Roberts G., 1988, MNRAS, 234, 755
Ezuka H., Ishida M., Makino F., 1998, ApJ, 499, 388
Feast M. W., Robertson B. S., Catchpole R. M., 1977, MNRAS, 179, 499
Feast M. W., Glass I. S., Whitelock P. A., Catchpole R. M., 1989, MNRAS, 241, 375
Fireman G., Imhoff C., 1989, IUE NASA Newsl., 40, 10
Fleming W. P., 1912, Ann. Harvard College Obs., 56, 165
Gallagher J. S., Holm A. V., Anderson C. M., Webbink R. F., 1979, ApJ, 229, 994
Girard T., Willson L. A., 1987, A&A, 183, 247
Glass I. S., Whitelock P. A., Catchpole R. M., Feast M. W., 1995, MNRAS, 273, 383
Haniff C. A., Scholtz M., Tuthill P. G., 1995, MNRAS, 276, 640
Harries T. J., Howarth I. D., 1996, A&AS, 119, 61
Hayes D., Latham D., 1975, ApJ, 197, 593
Henize K. G., 1976, ApJS, 30, 491
Herbig G. H., 1993, ApJ, 407, 142
Hollis J. M., Oliversen R. J., Kafatos M., Michalitsianos A. G., 1986, ApJ, 301, 877
Holm A., Bohlin R. C., Cassatella A., Ponz D., Schiffer F. H., 1982, A&A, 112, 341
Iben I., Tutukov A. V., 1996, ApJS, 105, 145
Imhoff C., Wasatonic R., 1986, IUE NASA Newsl., 29, 45
Ivison R. J., Seaquist E. R., 1994, MNRAS, 268, 561 (IS94)
Josafatsson K., Snow T. P., 1987, ApJ, 319, 436
Kafatos M., Lynch J. P., 1980, ApJS, 42, 611
Kafatos M., Michalitsianos A. G., Feibelman W. A., 1982, ApJ, 257, 204 (K82)
Kafatos M., Michalitsianos A. G., Fahey R. P., 1985, ApJS, 59, 785 (K85)
Karovska M., Hack W., Raymond J., Guinan E., 1997, ApJ, 482, L175
Kato M., 1997, in Mikołajewska J., ed. Physical Processes in Symbiotic Binaries and Related Systems. Copernicus Foundation for Polish Astronomy, Warsaw, p. 65
Keenan F. P., Johnson C. T., Kingston A. E., 1988, A&A, 202, 253
Keenan F. P., Aller L. H., Hyung S., Conlon E. S., Warren G. A., 1993, ApJ, 410, 430
Keenan F. P., Aller L. H., Hyung S., Brown P. J. F., 1995, PASP, 107, 148
Kenyon S. J. 1986, The Symbiotic Stars. Cambridge Univ. Press, Cambridge
Kenyon S. J., Fernandez-Castro T., 1987, AJ, 93, 938
Kenyon S. J., Fernandez-Castro T., Stencel R. E., 1988, AJ, 95, 1817
Kenyon S. J., Oliversen N. A., Mikołajewska J., Mikołajewski M., Stencel R. E., Garcia M. R., Anderson C. M., 1991, AJ, 101, 637
Kenyon S. J., Mikołajewska J., Mikołajewski M., Polidan R. S., Slovak M. H., 1993, AJ, 106, 1573
Klutz M., 1979, A&A, 73, 244
Klutz M., Swings J. P., 1981, A&A, 96, 406
Klutz M., Simonetto O., Swings J. P., 1978, A&A, 66, 283
Livio M., 1988, in Mikołajewska J., Friedjung M., Kenyon S. J., Viotti R., eds, The Symbiotic Phenomenon. Kluwer, Dordrecht p. 149
Mattei J. A., 1997, J. AAVSO, 25, 57
Michalitsianos A. G., Kafatos M., Hobbs R. W., 1980, ApJ, 237, 506
Michalitsianos A. G., Kafatos M., Fahey R. P., Viotti R., Cassatella A., Altamore A., 1988, ApJ, 331, 477
Michalitsianos A. G., Kafatos M., Meier S. R., 1992, ApJ, 389, 649
Mikołajewska J., 1994, in Shafter A. W., ed., ASP Conf. Ser. Vol. 56, Interacting Binary Stars. Astron. Soc. Pac., San Francisco, p. 374
Mikołajewska J., Kenyon S. J., 1992a, AJ, 103, 579
Mikołajewska J., Kenyon S. J., 1992b, MNRAS, 256, 177
Mikołajewska J., Mikołajewski M., Biernikowicz R., Selvelli P. L., Turło Z., 1987, in Appenzeller I., Jordan C., eds, Circumstellar Matter. Reidel, Dordrecht, p. 487
Mikołajewska J., Selvelli P. L., Hack M., 1988, A&A, 198, 150
Mikołajewska J., Kenyon S. J., Mikołajewski M., Garcia M. R., Polidan R. S., 1995, AJ, 109, 1289
Mikołajewska J., Acker A., Stenholm B., 1997, A&A, 327, 191
Müller B. E., Nussbaumer H., 1985, A&A, 145, 144

Munari U., Whitelock P. A., 1989, MNRAS, 237, 45P
Munari U., Zwitter T., 1997, A&A, 318, 269
Munari U., Yudin B. F., Taranova O. G., Massone G., Marang F., Roberts G., Winkler H., Whitelock P. A., 1992, A&AS, 93, 383
Mürset U., Nussbaumer H., 1994, A&A, 282, 586
Mürset U., Wolff B., Jordan S., 1997, A&A, 319, 201
Neckel, Th., Klare G., 1980, A&AS, 42, 251
Netzer H., 1975, MNRAS, 171, 395
Nota A., Jedrzejewski R., Voit M., Hack W., 1996, FOC Instrument Handbook V7.0. Space Telescope Science Institute, Baltimore
Nussbaumer H., 1982, in Friedjung M., Viotti R., eds, The Nature of Symbiotic Stars. Reidel, Dordrecht, p. 85
Nussbaumer H., Storey P. J., 1978, A&A, 70, 37
Nussbaumer H., Storey P. J., 1979, A&A, 71, L5
Nussbaumer H., Storey P. J., 1981, A&A, 99, 177
Nussbaumer H., Storey P. J., 1982, A&A, 115, 205
Nussbaumer H., Storey P. J., 1984, A&AS, 56, 293
Nussbaumer H., Vogel M., 1990, A&A, 236, 117
Nyman L.- Å., Olofsson H., 1986, A&A, 158, 67
Orio M., 1993, A&A, 274, L41
Paczyński B., 1970, Acta Astron., 20, 47
Paresce F., 1990, ApJ, 357, 231
Patterson J., Raymond J. C., 1985, ApJ, 292, 535
Payne-Gaposchkin C., Gaposchkin S., 1938, Variable Stars. Harvard Univ. Press, Cambridge, MA
Pickering E. C., 1897, Circ. Harv. Coll. Obs., 17
Pickering E. C., 1914, Circ. Harv. Coll. Obs., 182
Prialnik D., Kovetz A., 1995, ApJ, 445, 789
Proga D., Mikołajewska J., Kenyon S. J., 1994, MNRAS, 268, 213
Proga D., Kenyon S. J., Raymond J. C., Mikołajewska J., 1996, ApJ, 471, 930
Reimers D., Cassatella A., 1985, ApJ, 297, 275
Sanduleak N., Stephenson C. B., 1973, ApJ, 185, 899
Schmid H. M., 1996, MNRAS, 282, 511
Schmid H. M., Schild H., 1990a, MNRAS, 246, 84
Schmid H. M., Schild H., 1990b, A&A, 236, L13
Schönberner D., 1989, in Torres-Peimbert S., ed., Planetary Nebulae. Kluwer, Dordrecht, p. 463
Schulte-Ladbeck R. E., 1988, A&A, 189, 97
Schwarz H. E., Nyman L.- Å., Seaquist E. R., Ivison R. I., 1995, A&A, 303, 833
Seaton M. J. 1979, MNRAS, 187, 73P
Seaquist E. R., Taylor A. R., 1987, ApJ, 312, 813
Seaquist E. R., Taylor A. R., 1992, ApJ, 387, 624
Seaquist E. R., Taylor A. R., Button S., 1984, ApJ, 284, 202 (STB84)
Seaquist E. R., Krogulec M., Taylor A. R., 1993, ApJ, 410, 260
Selvelli P. L., Cassatella A., Gilmozzi R., 1992, ApJ, 393, 289
Sembach K. R., Danks A. C., Savage B. D., 1993, A&AS, 100, 107
Sion E. M., 1997, in Mikołajewska J., ed., Physical Processes in Symbiotic Binaries and Related Systems. Copernicus Foundation for Polish Astronomy, Warsaw p. 49
Smak J., 1964, ApJS, 9, 141
Snow T. P., York D. G., Welty D. E., 1977, AJ, 82, 113
Stone R. P. S., Baldwin J. A., 1983, MNRAS, 204, 347
Swings J. P., Klutz M., 1976, A&A, 46, 303
Swings P., Struve O., 1941, ApJ, 94, 291
Uus U. H., 1970, Nauchn. Inf., 17, 48
van Leeuwen F., Feast M. W., Whitelock P. A., Yudin B., 1997, MNRAS, 287, 955
van Winckel H., Duerbeck H. W., Schwarz H., 1993, A&AS, 102, 401
Wallerstein G., 1986, A&A, 163, 337
Webbink R. F., Livio M., Truran J. W., Orio M., 1987, ApJ, 314, 653
Webster B. L., Allen D. A., 1975, MNRAS, 171, 171
Whitelock P. A., 1987, PASP, 99, 573
Whitelock P. A., 1988, in Mikołajewska J., Friedjung M., Kenyon S. J., Viotti R., eds, The Symbiotic Phenomenon. Kluwer, Dordrecht, p. 47
Whitelock P. A., 1999, in Takeuri M., Sasselov D., eds, Pulsating Stars – Recent Developments in Theory and Observation. Universal Academy Press, Tokyo, in press (astro-ph/9710032)
Whitelock P. A., Catchpole R. M., Feast M. W., Roberts G., Carter B. S., 1983a, MNRAS, 203, 363 (W83)
Whitelock P. A., Feast M. W., Catchpole R. M., Carter B. S., Roberts G., 1983b, MNRAS, 203, 351
Whitelock P. A., Menzies J. W., Lloyd Evans T., Kilkenny D., 1984, MNRAS, 208, 161 (W84)
Whitelock P. A., Menzies J., Feast M., Marang F., Carter B., Roberts G., Catchpole R., Chapman J., 1994, MNRAS, 267, 711
Whitelock P. A., Feast M. W., Marang F., Overbeek M. D., 1997, MNRAS, 288, 512
Yamamoto I., 1924, Bull. Harv. Coll. Obs., 809
Yudin B., Munari U., Taranova O., Dalmeri, I., 1994, A&AS, 105, 169

This paper has been typeset from a TEX/LATEX file prepared by the author.